Hardware and Software Integration and Testing for the Automation of Bright-Field Microscopy for Tuberculosis Detection

by

Devi Krishna Sarala

A thesis submitted to the University of Cape Town
in partial fulfilment of the
requirements for the degree of
MSc (Med)
in
BIOMEDICAL ENGINEERING

Faculty of Health Sciences
University of Cape Town
February 2011

Supervisor: Associate Professor Tania S Douglas

Declaration

I, Devi Krishna Sarala, hereby declare that the work on which this dissertation is based, is my original work (except where acknowledgements indicate otherwise).

This work is being submitted for the Master of Science (Med) in Biomedical Engineering at the University of Cape Town. It has not been submitted to any other university for any other degree or examination. I empower the university to reproduce for the purpose of research either the whole or any portion of the contents in any manner whatsoever.

Signature: …….....

Date: ……...

Acknowledgements

I would like to thank Associate Professor Tania Douglas, my supervisor, for all her enthusiastic guidance and efficient advice during my Masters project.

I also thank Mr Sriram Krishnan, who provided many useful insights and made several suggestions that contributed to the outcome of the project.

Thanks, also, to Ronald Dendere and Rethabile Khutlang.

Thanks to all the staff members especially to Rachel, Sam, Yunous, at the TB lab in the National Health Laboratory Services for providing the sputum slides and for their assistance in labelling bacilli in Ziehl-Neelsen stained sputum images.

Thanks to Susan Cooper for her assistance and for providing access to the Zeiss microscopy imaging unit in the Department of Human Biology.

Thanks to all my colleagues, friends and family members for their kind support.

Abstract

Automated microscopy for the detection of tuberculosis (TB) in sputum smears would reduce the load on technicians, especially in countries with a high TB burden. This dissertation reports on the development and testing of an automated system built around a conventional microscope for the detection of TB in Ziehl-Neelsen (ZN) stained sputum smears. Microscope auto-focusing, image analysis and stage movement were integrated. Images were captured at 40x magnification.

Algorithms for auto-focusing, image segmentation and object classification developed by other researchers were evaluated. Auto-focusing on fields of ZN-stained sputum smears was performed by Vollath's F_4 measure. Pattern recognition was performed for the identification of bacillus objects in images of ZN-sputum smears. A quadratic pixel classifier was used for the segmentation of objects of interest from their background. Classification of segmented objects as bacilli or non-bacilli was achieved by the kNN classifier. Bacillus detection was achieved with a sensitivity of 98.3% and specificity of 94.5%, on a per bacillus basis. On a per image basis, 97.5% sensitivity and 96.6% specificity were achieved.

The steps from capturing an image to the classification of a slide as positive or negative were integrated and automated, taking into account the characteristics of the mechanical stage of the microscope. A graphical user interface (GUI) was developed along with the integration algorithm. The automated system was evaluated on a per slide basis and achieved sensitivity of 92% and specificity of 89%.

Smear thickness inconsistency on slides affected the performance of the algorithms and the system. The inter-dependency of algorithms created difficulties because, if one function failed, it would affect the performance of consecutive functions. Hardware limitations that were observed during the integration of the software resulted in a longer processing time than expected. On a per field basis, the automated system gave acceptable performance for TB detection in ZN-stained sputum smears, but practical implementation of the overall automated system is not yet feasible.

Contents

List of Tables

List of Figures

1. Introduction

1.1 Background to study

Tuberculosis (TB) affects more than 10 million people each year. The World Health Organisation (WHO) declared this infectious disease a global emergency in 1993. In 2008, 1.8 million people died from TB i.e. 4500 deaths per day (World Health Organization, 2009b). The WHO estimates that 36 million more people will die from TB by the year 2020, unless diagnostic methods, control and prevention are improved (Global Health Initiative, 2007).

Although it is a worldwide threat, the highest incidence rates occur in developing countries: South Africa ranked third and Nigeria fourth, in terms of the total number of TB cases in 2008, only overtaken by India and China. Furthermore, TB contributes to the high mortality rate of HIV infected patients in these areas (World Health Organization, 2009a).

It is essential to have timely and accurate diagnosis of TB to improve treatment, reduce transmission and to control the development of drug resistance. In low- and middle income countries, microscopy is the cornerstone of TB screening, even though such screening is labour intensive and has variable sensitivity (Steingart et al., 2006). Inadequate equipment, few skilled technicians and high caseloads at limited numbers of microscopy labs are the setbacks faced in these countries. Manual interpretation of slides also leads to a high false-negative rate, as a result of the visual strain and mental fatigue caused by the task. Automation of sputum-smear microscopy for TB detection aims to accelerate the screening process, improve its sensitivity and minimise its reliance on technicians.

Many microscope functions have been automated in recent years in order to reduce the manual workload required for various applications. Though the design of the widely used bright field microscope has remained more or less the same over the years, automation processes are advancing: image-processing techniques and decision-making tools have improved considerably with software development. Automation of microscope functions for the detection of TB remains an area to which little attention has

been paid; in recent years research has been published on the detection of TB bacilli in sputum smears images (Forero et al., 2006; Khutlang et al., 2010; Sadaphal et al., 2008 and Veropoulos et al., 1999). However these studies do not deal with a complete system for TB detection.

The aim of this project described is to develop a complete system for automatic TB detection in Ziehl-Neelsen (ZN) stained sputum smears. The focus will be on the selection and implementation of algorithms for auto-focusing and pattern recognition of TB bacilli in digital images of sputum smears, which were proposed by various researchers, their integration with electromechanical components attached to a microscope, and an evaluation of overall system performance.

1.2 Objectives

The objectives of the study were to:

- train image segmentation and classification algorithms proposed by Khutlang (2009), to extract and identify candidate bacillus objects in digital images of fields of ZN-stained sputum smears obtained from a Nikon55i microscope with 40x magnification;
- analyse an area of the slide equivalent to the WHO standard of 100 fields for 100x magnification;
- implement the auto-focusing algorithm suggested by Osibote et al. (2010) on the microscope;
- integrate auto-focusing and classification software with the microscope and create a user-friendly graphical user interface to run the integrated system; and
- evaluate the performance of the algorithms, the hardware and finally the integrated system

1.3 Thesis outline

Chapter 2 provides an overview of TB and microscopy.

Chapter 3 presents a literature review on automatic detection of TB in sputum smears.

Chapter 4 describes the tools and materials used in the study.

Chapter 5 describes the methods used for auto-focusing and pattern recognition.

Chapter 6 presents the results of pattern recognition methods.

Chapter 7 presents the hardware testing performed and the results obtained.

Chapter 8 presents the integration methods.

Chapter 9 presents the results of integration.

Chapter 10 provides a discussion on the results obtained and draws overall conclusions. Recommendations for future work are also made.

2. Overview: Tuberculosis and Microscopy

This chapter gives a brief description of TB the disease, and the light microscope, the instrument being automated in this study for the identification of TB in ZN-stained sputum smears.

2.1 Tuberculosis

TB is an easily transmissible disease, mainly attacking the lungs although it can spread to the nervous system, skin, bone, genitals and kidneys, among various other parts of the body. It is caused by rod-shaped non-motile micro-organisms as shown in Figure 1, called *Mycobacterium tuberculosis* (Todar, 2009). A person may be infected and be a silent carrier of TB by having the TB bacteria in the body, without symptoms, as the immune system has the bacteria under control (Luna, 2005). Symptoms of the disease include a chronic cough, fever, chest pain, night sweats, loss of appetite, fatigue, presence of blood in sputum and weight loss (Todar, 2009). The symptoms of the disease are experienced when the latent infection evolves into active TB. In low income countries the spread of TB has been worsened by co-infection with HIV/AIDS.

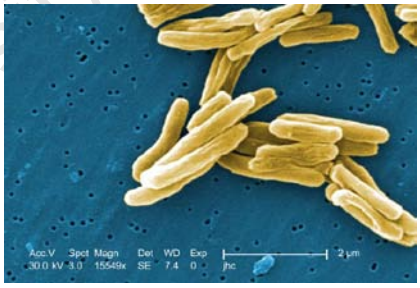

Figure 1: Mycobacterium tuberculosis (Todar, 2009)

2.2 Sputum smear microscopy

Early and accurate detection of TB is necessary for efficient control of the disease.

Sputum smear microscopy is a simple, rapid and reliable identification technique for active TB. It is the principal bacteriologic examination for TB diagnosis and monitoring (Steingart et al., 2006).

Sputum is a mucus-like secreted substance that can be coughed up from the lungs. The sputum of a TB infected person contains bacilli of *Mycobacterium tuberculosis*. These *M. tuberculosis* are the object of interest in this dissertation. Bacilli can have a width between 0.2 and 0.6µm and a length between 1 and 10µm exhibiting a straight, curved or bent shape (see reddish objects in Figure 2) (Forero et al., 2006). Owing to their non-permeability to certain dyes and stains, tuberculosis bacilli are classified as acid-fast bacteria (AFB). When heated and treated with acidified organic compounds, acid-fast bacteria retain the dyes. Sputum samples are smeared onto slides and stained, using either an auramine/rhodamine stain or a ZN-stain, yielding monochrome (fluorescent) or colour images, respectively. The auramine stain causes the bacilli to fluoresce against a dark background. The ZN-stain causes the bacilli to retain a red colour and the specimen is counterstained with methylene blue to make the background appear blue as shown in Figure 2. A simple light microscope is used to view slides of ZN-stained sputum to detect the reddish pink bacilli against a blue background.

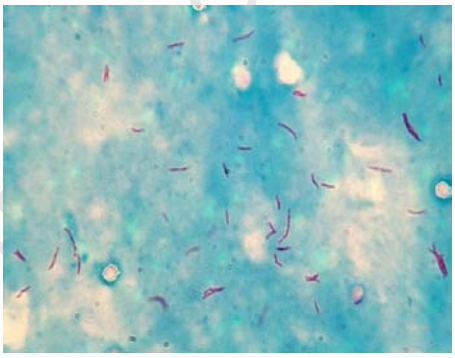

Figure 2: ZN-stained sputum smear

Steingart et al. (2006) concluded after reviewing a number of studies that fluorescence microscopy has higher sensitivity, and similar specificity compared to bright field microscopy, for TB screening. Capital costs associated with fluorescence microscopy have decreased recently with the introduction of fibre optic-based, light emitting diode-based systems (Steingart et al. 2006). However, since fluorescent microscopes have, until recently, been more expensive and complex and not affordable to many laboratories in poor and developing nations, these laboratories still continue to use ZN-light

microscopy. ZN microscopy is the primary diagnostic strategy that is recommended by the WHO (WHO, 1998) for active tuberculosis worldwide.

2.3 Classification of tuberculosis infection

A sputum smear can be classified based on the number of bacilli identified per microscope field which is also an indication of the severity of the disease. The standard scale set by the WHO when using 100x magnification is given in Table 1 (WHO, 2002).

Table 1: Grading of ZN-sputum smear microscopy results

Number of bacilli	Recording	Clinical result
0 AFB per 100 fields	Negative	Negative
1-9 AFB per 100 fields	Record exact figure	Positive
10-99 AFB per slide	1+	Positive
1-10 AFB in each field	2+	Positive
>10 AFB in each field	3+	Positive

A 100x oil immersion objective is normally used by a technician to examine ZN-slides. The average number of ZN-slides that a technician examines in a day varies from 30 to 40 (Toman, 2004). Generally, a set number of fields on a slide are viewed by the technician to conclude whether the slide is smear positive or negative. According to WHO standards (World Health Organization, 2003), a technician should examine 100 fields (when using a 100x lens) before concluding the smear is negative. However, if bacilli are sparse in a slide, as is often the case with HIV co-infection and in sputum obtained from children, there are chances that they may conclude a positive slide as negative.

2.4 Microscopy

2.4.1 Standard light microscope

A microscope with total magnification between 400x and 1000x is used to detect TB bacilli (Hanscheid, 2008). Magnification is described as the ratio of image size to object

size. In other words, it is the degree of enlargement of detail presented. A simple microscope has an objective lens and an eyepiece, and therefore the magnification produced is the product of magnification by the objective and eyepiece lenses. In standard microscopes, objective lens magnifications range from 4x to 100x. Eyepieces generally have a magnification of 10x.

It is essential to have uniformity of light to avoid shadows, glare and inadequate contrast especially when capturing magnified images of a specimen through a microscope. To evenly illuminate the specimen, the Köhler illumination method is used in light microscopes. Köhler illumination consists of a collector lens that focuses light at the condenser diaphragm, which in turn provides for parallel and evenly distributed illumination of the specimen (Olympus, 2010a).

2.4.2 Light and optics

The refraction or bending of light affects the magnification and resolution abilities of a microscope. Light refracts when it passes from one medium to another of different optical density. Lenses have two or more refracting surfaces of which at least one is curved. In an optical system, lenses are used to modify a beam of light or to produce an image of an object (Olympus, 2010a). Some of the features of the optical system of a light microscope, that may be important to know for this thesis, are described here.

a) Focal Length

The parallel rays coming into the lens from a far-away object (object at 'infinity') converge at a point called the focal point. The distance from this point to the centre of the lens is the focal length *f* of a thin/simple lens. A system with shorter focal length has higher optical power and vice versa. Optical power is the degree to which a lens (or optical system) converges or diverges the light and is equal to $\frac{1}{f}$. However, typical microscope objectives contain compound lens (a combination of simple lens). Therefore the resulting focal length of an objective is called effective focal length and it is smaller than the focal length of any of the lens by themselves.

b) Numerical Aperture (NA)

The NA of a microscope objective is a measure of its ability to gather light and thus its ability to resolve fine specimen detail at a fixed objective distance. It is calculated using the following formula (Olympus, 2010b):

$$NA = n * (\sin \mu)$$

where n is the refractive index of the medium between the front lens of the objective and the specimen. $n = 1$ for air. μ is one-half angular aperture. The bigger the μ, the higher the numerical aperture. The theoretical maximum value of NA is 1, when the medium is air (Olympus, 2010b).

c) Depth of Field

The depth of field of an optical system is the range of distance along the optical axis in which the details of the sample appears 'in-focus' (Geusebroek et al., 2000). Depth of field can be calculated from the equation given here (Young et al., 1993; Geusebroek et al., 2000):

$$D.o.F = \frac{\lambda}{2n(1 - \sqrt{1 - (\frac{NA}{n})^2})}$$

where n is the refractive index of the medium, λ is the wavelength of the light used and NA is the numerical aperture of the objective lens.

Microscopy samples are often relatively thin, in the order of a few micrometers, and the depth of field of high power objectives typically used for imaging is even smaller (Yazdanfar et al., 2008). Therefore, the distance between the sample and objective must be dynamically changed according to variations in the sample to maintain the sample at optimal focal position. Figure 3 below illustrates the depth of field across a TB slide.

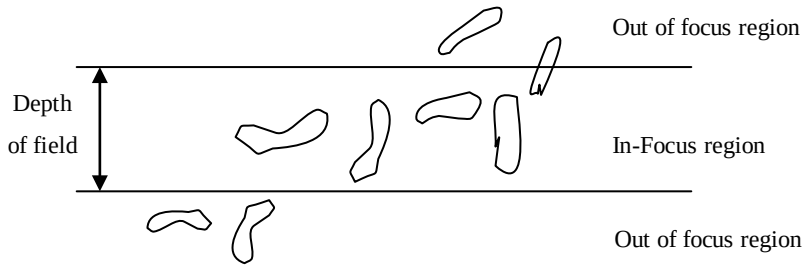

Figure 3: Depth of Field- Illustration of a cross section through a TB sputum slide

2.5 Computerised/automated microscopy applications

The applications of automated microscopy range from optimising the simple but tedious task of cell counting to the accurate detection of diseases in the microscopic, pre-surgical stages. A few such applications are given here.

For the early detection of lung cancer, bronchioalveolar lavage (BAL) samples are microscopically examined to detect the rare and low probability tumour cells. Ortiz-de-Solorzano et al. (2008) automated a multi-spectral microscopy system for the unsupervised detection of rare cancerous candidate cells and 3-D analysis of genomic integrity. Multi-spectral microscopy combines images taken with light of specific wavelengths for enhanced light-microscopic imaging and is enabled by coupling spectral imaging systems to traditional microscopes in a system configuration (Thigpen et al., 2010).

Palynology or pollen analysis is the recognition and counting of the types of pollen present in slides using a microscope. Allen et al. (2006) automated a low-cost, trainable microscope system for the recognition and counting of pollen. This system incorporates an auto-focus system, digital cameras, segmentation software, image feature selection and classification, and an x- y- stage that allows slides to be scanned. The system finds pollen grains on a slide. Features are extracted and used for the classification of different types of pollen and gives the count of each pollen type. These classification results can be manually checked.

The AutoPap screening system is used to aid and speed up the identification of cervical cancer cells. It uses a high resolution scanner and a high speed video microscope to obtain cell images from conventional Pap smears. Digital images are analysed by specially designed algorithms to identify high probability cases. Slides reported as having lowest probability of being abnormal can be safely excluded without further manual cytologist review. Cases that meet the highest probability criteria of containing abnormal cells are further screened manually by cytologists, thus reducing the time spent on viewing normal slides (Chang et al., 2002).

Renal and urinary tract diseases can be tracked by microscopic examination of urine sediment. The iQ200 is an automated urine microscopy analyser that uses digital

imaging and a trained neural network to classify and quantify cells in uncentrifuged urine. Extracted features such as size, shape, contrast and texture are used by the neural network pattern recognition software for classification of particles (Wah et al., 2005).

2.6 Steps in automated microscopy

This section outlines the general steps (Figure 4) required in automated microscopy to identify objects such as TB bacilli. The components of a typical automated microscopy system consists of a digital camera, motorized stage, focus motor, image analysis software and a user interface.

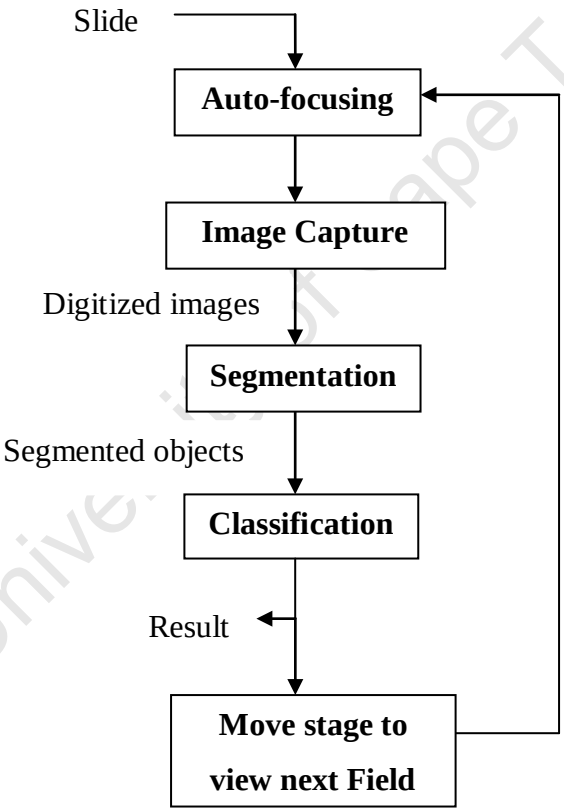

Figure 4: Typical automated microscopy system overview

The first step in microscopy is focusing the field of view for clear vision. A digital image of the field of view is acquired once in focus. In order to use a digital camera with a microscope, the microscope must have a port for the camera and a suitable illumination system (Floyd, 1998). A computer is used for camera control, for other function controls

and for the storage of images. Image capture can be facilitated by the software that comes with the camera attachment. An image corresponds to a field of view captured by the camera.

An image contains a lot of information which may not be of any interest to the study. Separate entities in the images are referred to as objects. Segmentation decreases the content in an image by extracting only the objects of interest from the background (Khutlang, 2009). Segmented images have much less content when compared to the original image. The extracted objects from a segmented image are classified using a classifier.

Once an image has been examined, the stage is moved, with respect to the objective, to capture an image of the next field. The same process of focusing, segmentation and classification is repeated for the desired number of fields. Typically, motors incorporated in the system control the stage movement that effects field to field movement and focusing. Stage control is described in the next section.

2.6.1 Stage control

Conventionally, the horizontal plane is denoted by x- y- (with no particular preference for the axes) and the vertical axis is denoted as the z-axis. Movement along the x- and y-axes changes the field of view whereas movement along the z-axis is for focusing the slide. Along the z-axis, a coarse movement knob facilitates larger steps and a fine movement knob facilitates minute steps towards focusing. Stage control, i.e. x-, y- and z-axes movement can be facilitated using servomotors or stepper motors.

A servomotor is an electromechanical device in which an electrical input determines the position of the armature of a motor. It uses error-sensing negative feedback to correct the performance of the system. A servomotor can offer a precise and highly repeatable platform for demanding microscopy applications (Applied Scientific Instrumentation, 2003). Servomotors provide position feedback and are used in high performance microscopes when a very high degree of accuracy is needed. The actual stage position with respect to a point of reference can be displayed when servomotors are used.

Stepper motors do not have position feedback. One of the main differences in the operation of servomotor from stepper motor is that servomotors run using a control loop

and use feedback from the motor to help the motor to get to the desired position (Jerome, 2010). When a stepper motor misses a step, there is no control loop to compensate for the missed step. Servomotors run more smoothly than stepper motors except when micro-stepping is used. However, servomotors are more expensive than stepper motors, cannot work in an open loop, and require feedback, tuning of control loop parameters, and more maintenance (Jerome, 2010). Therefore, stepper motors are a low-cost alternative to servomotor position controls.

A few examples in which microscopy stage control was performed are given below.

Hatiboglu et al. (2004) used two servomotors, a controller chip and Java-based image processing software to control the movements of a microscope stage in the application of petrographic analysis of sedimentary rocks. In this design, the first servomotor ensured action in the y-axis but it also influenced the orthogonal axis, thus producing error. The other servomotor that was responsible for the orthogonal action corrected this error with the help of software.

Macedo et al. (2005) used T-LA28 linear actuators from Zaber Technologies Inc. for the control of each axis of the translation stage in their application of obtaining 3-D images in wide-field microscopy. The actuator they used incorporated stepper motor controller and driver. The linear resolution for this linear actuator was approximately 0.0992µm.

McKeogh et al. (1995) built a low cost automated stage control and focus system for the application of assembling a database of images of cellular material from Pap smears. In their design, stepper motors are attached to the microscope focus and translation stage controls. A maximum speed of about 500µms^{-1} was achieved for the stage motion.

The choice of the xyz stage control motor depends on what application the stage is used for. Factors like motor drive, feedback, cost, resolution and repeatability are considered.

2.7 Evaluation of the microscope/hardware stage

Van den Doel et al. (1998) performed characterisation of the stage on three high-end microscopes. They measured the planar x- and y- motion of the Ludl (stepper motor) motorized stage of Zeiss axioskop and Marzhauser stepper motor of Leitz Aristoplan to measure the hysteresis of the stepper motors. They sent the stage back and forth over an increasing distance, Δx, and measured the error between the defined distance and the

measured distance. They used a test slide referred to as HCM slide in their study that had a grid of fiducial marks for measurements. An average of 0.37µm and 1.2µm hysteresis was found for both respectively.

To examine the hysteresis in the z-axis, Van den Doel et al. (1998) assessed the focus function while the stage was moving in the positive and negative directions. A graph of the focus function against the z-position was then plotted for both directions. The shift in the peaks of the two plots represented the hysteresis of the motor. The Zeiss Axioplan gave a negligible shift whereas the other two microscopes had a distinguishable shift.

McKeogh et al. (1995) used a conventional microscope with stepper motors to actuate the stage in their application of assembling a database of images from Pap smears. To determine the x- y- stage accuracy, they sent the stage to a random position from a given starting point and returned it to the starting point to determine how closely the stage returned to the starting point. The stage they tested had an accuracy of approximately 50µm (they do not mention how the accuracy was measured). The inaccuracy was due to backlash in the microscope and laxity in the gearing components.

Van den Doel et al. (1998) assessed the axial position surface, z(x, y), by measuring the in-focus position along the x- y-axis. They moved the stage along every fiducial mark on the HCM slide and measured the focus position of every mark. They obtained a z-range of 60µm for all three microscopes.

The automated system by McKeogh et al. (1995) had to be positioned near to focus at start-up and the system was liable to drift very far away from focus when the object plane became empty.

2.8 Integration

Software and hardware integration into a well-coordinated, efficient system is a challenging task (Floyd, 1998). Interfacing units that independently function correctly may give problems when interfacing and may cause failures at this stage (Pressman, 2005). Holdaway (2004) performed microscope integration in his application, to capture images of microscopically magnified pollen, segment them and classify the type of pollen. Human input can be provided by an operator where it is extremely difficult to automate or where the system can be greatly simplified by this input (Holdaway, 2004).

Allen et al. (2006) built an x- y- stage and focus hardware and developed segmentation and focus algorithms for automated microscopic classification of pollen grains on a slide. A portion of a slide to be processed was selected by a user. A count of the number of each type of pollen grain was achieved in their study. In their hardware design, a standard microscope slide holder held the slide and the x- y- stage was moved by two stepper motors. The area viewed by the high magnification camera was 429µm x 319.8µm. They had two settings in the same microscope: a low magnification with a large field of view to locate pollen grains quickly, and a high magnification setting to capture images with sufficient detail for feature extraction. The camera sensor elements they used were 4.65 microns square. Their method required the low magnification camera to be manually focused initially. Also, it needed the user to set the limits for a region of interest within the total area of the slide. The higher magnification obtained with the cameras enabled the use of a small optical magnification (10x) which in turn resulted in a depth of field greater than that of a conventional microscope. Therefore, the focus position found could be retained throughout the slide. The process from auto-focusing to saving the image of pollen captured took 15s in their study.

The literature on microscope integration is limited. Some researchers use an open source package that includes a user interface for integrating their software components. In the application of Hatiboglu et al. (2004), the moving stage controller software was integrated into freely available image processing software called ImageJ (ImageJ, 2009). There are numerous publicly available stand-alone tools for image analysis such as segmentation, feature selection, classification but they are often application-specific and may require programming effort for their integration. In addition, most of these software options are not well integrated and user-friendly (Shamir et al., 2010). Also, if the original authors abandon the software project without providing the source code, then the software may soon stop running on new versions of operating systems and hardware (Shamir et al., 2010).

3. Review: Automated Bacillus Detection

This chapter reviews methods that may be appropriate for the automatic detection of bacilli at 40x magnification in an automated microscope solution.

3.1 Auto-focusing

Auto-focusing ensures, by automatic methods, that a microscopy specimen is in correct focus for clear viewing. Auto-focusing can be achieved in two forms, namely, passive auto-focusing and active auto-focusing (Nicolls, 1995). In the former, the value of a pre-defined focus measure is found in images captured at different positions of the lens with respect to the slide. The best focused image is searched for from the focus measure values. This method is computationally expensive as it requires a search algorithm to go through different lens positions to capture images in order to find the position of focus (Subbarao and Tyan, 1998).

Active auto-focusing uses knowledge of the image formation process to find the degree of defocus of an object in an image (Nicolls, 1995). The information on the amount of defocus of an object is used to determine the distance to the object. With this distance found, the focal length can be corrected to bring the object into focus. In active auto-focusing, the advantage is that the entire search process associated with passive focusing can be eliminated (Russell and Douglas, 2007). However, look-up tables or models containing the system parameters are required for the translation of the amount of blur into the distance to the object. Another requirement is for the system to be calibrated before the calculation of the distance to the object (Nicolls, 1995). Also, according to Subbarao and Tyan (1998), active auto-focusing methods are less accurate than passive auto-focusing methods.

A passive auto-focus algorithm has two components: 1) the focus measure and 2) the search algorithm.

3.1.1 Focus measure

The focus measure indicates how in-focus an image is. It is generally based on the illumination gradient of an image (Malik and Choi, 2008). The image is first normalised for brightness and then convolved with a focus measure filter (FMF). The energy (sum of squared values) in the resultant filtered image is the focus measure, which is then computed (Figure 5). The majority of FMFs correspond to filters that amplify (emphasise) high frequencies. As the image sharpness increases, the focus measure value increases, therefore focus measures are generally Gaussian in shape as shown in Figure 6. An ideal focus algorithm calculates a maximum value for the focus measure at the most focused image (Huang and Jing, 2007; Sun et al., 2004).

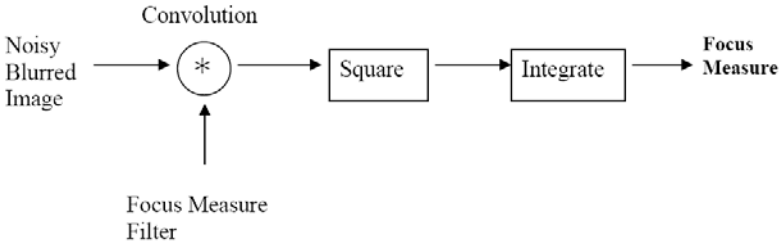

Figure 5: Model of a focus measure calculation (Subbarao and Tyan, 1998)

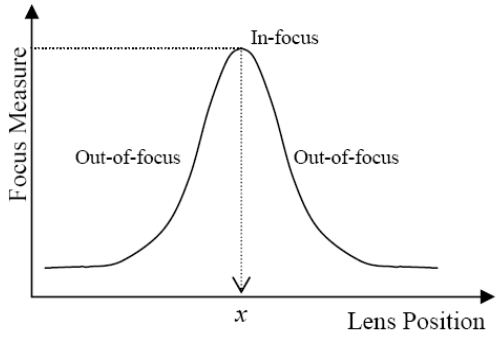

Figure 6: Example of an ideal focus measure curve (Russell and Douglas, 2007)

A focus measure is typically selected using the criteria given below (Sun et al., 2004; Huang and Jing, 2007).

1. The focus measure must have only one maximum.
2. The system must be in focus at the maximum.

3. The range which describes the distance between two neighbouring local minima around the global maximum over which an in-focus image can be attained must be as large as possible.
4. The focus measure must not be limited to some special types of images.
5. The focus measure must be robust to noise.
6. The focus measure must be easy to implement and fast.

Previous researchers, Russell and Douglas (2007) and Osibote et al. (2010) examined auto-focusing algorithms for bright-field microscopy of ZN-stained sputum smears. Russell and Douglas (2007) selected focus measures published for microscopy applications that might be suitable for ZN-stained sputum slides: energy of the image Laplacian, variance of the log-histogram and first order Gaussian derivative were evaluated. The variance of the log-histogram focus measure-plots gave a poor shape and were not unimodal. The energy of the image Laplacian focus measure-plots gave an acceptable shape similar to that of the first order Gaussian derivative, although the latter displayed a smoother and better shape. However, Russell and Douglas (2007) selected the energy of the image Laplacian focus measure as it took significantly less computing time than the first order Gaussian derivative. It also performed well with differing amounts of image content (high, medium and low).

Osibote et al. (2010) compared six focus measures defined in the spatial domain which are reported to be suitable for a variety of biological and biomedical applications: the normalised variance, the Brenner gradient, the sum-modified Laplacian, energy of the image Laplacian, Vollath's F_4 and Tenegrad's focus measure. They were ranked with respect to accuracy, execution time, range, full width at half maximum of the peak and the presence of local maxima. They were also evaluated qualitatively by visual inspection.

The curve fit produced by Vollath's F_4 and the Brenner gradient ranked the best in the Osibote et al. (2010) study. The energy of the image Laplacian gave average results. The Brenner gradient gave the lowest mean processing time (4.69s). However, Vollath's F_4 gave the highest accuracy and best overall performance and gave the second lowest mean processing time (5.27s). Santos et al. (1997) also found Vollath's F_4 as the best overall focus measure in a comparison study.

3.1.2 Vollath's F_4 focus measure

Vollath's F_4 focus measure is based on the autocorrelation function (Vollath, 1988):

$$F_{Vollat\,h4} = \sum_{i=1}^{M-1}\sum_{j=1}^{N} I(i,j).I(i+1,j) - \sum_{i=1}^{M-2}\sum_{j=1}^{N} I(i,j).I(i+2,j)$$

where I is the pixel intensity at (i,j), M and N are the height and width of the image respectively. This focus measure provides good performance in the presence of noise (Osibote et al., 2010).

3.1.3 Auto-focus search algorithm

Once the focus measure is calculated for different positions of the lens with respect to the slide, the lens should be moved to the position of optimal focus, i.e. the position corresponding to the highest value of the focus measure. This process may be achieved by a search algorithm.

Osibote et al. (2010) reviewed different search methods proposed by different researchers (Svahn, 1996; Subbarao and Tyan, 1998 and Yazdanfar et al., 2008) for finding the position of optimum focus. The search methods proposed by Svahn (1996) (difference of signs method) and Subbarao and Tyan (1998) (Fibonacci or binary search) involve extensive and time consuming mechanical motion as the optimal position is scanned through multiple times. Therefore, in order to reduce focusing time, Osibote et al. (2010) proposed an auto-focusing method that follows a curve-fitting approach suggested by Yazdanfar et al. (2008).

The curve-fitting method proposed by Yazdanfar et al. (2008) reduces the number of images needed to locate the position of optimum focus and does not require acquisition of an image precisely at the focus position for the purpose of auto-focusing. This is achieved by capturing a few images and fitting a Gaussian to the focus measures of the images. The peak of the curve is taken as an estimate of the focal position.

Osibote et al. (2010) captured a full stack and performed a global search to find the optimal focus position for the first field in each slide. Such a comprehensive evaluation of the first field was carried out to avoid locating the position of optimal focus at a local minimum and propagating the associated error through the slide. They applied the curve

fitting mentioned in the previous paragraph to subsequent fields of the slide. However, instead of fitting a Gaussian to the focus measures, Osibote et al. (2010) note that fitting a quadratic to the logarithm of the focus measures produces a similar result. Using this technique requires a minimum of three images since at least n+1 data points are necessary to fit a polynomial of order n to any data.

3.1.4 Step size for image acquisition

The accuracy of the prediction of the focus position decreases as the distance from the focal position at which images are acquired for fitting increases. Santos et al. (1997) suggested a step size smaller than 1µm to achieve fine focus.

Osibote et al. (2010) used the relationship between the depth of field and the numerical aperture of a microscope objective to determine the step size for their application (Nikon MicroscopyU, 2010):

$$Depth\ of\ Field = \frac{\lambda \eta}{NA^2} + \frac{\eta e}{M(NA)}$$

where λ is the wavelength used, η is the refractive index of the medium between the sample and the lens, NA is the numerical aperture of the objective, M is the magnification, e is the smallest distance that can be resolved by a detector placed at the image plane.

The spatial distance that can be resolved by the sensor in the camera used in this project has to be at least twice the pixel size of the camera, taking the magnification into account, to satisfy the Nyquist sampling criterion (Geusebroek et al., 2000; Osibote et al., 2010).

$$e = \frac{2 * Pixel\ Size\ of\ camera}{Magnification}$$

Osibote et al. (2010) captured images at a step size apart from each other. They captured one image on one side from the focal position determined from the previous stack and two on the other side (which includes the previous focal position). Osibote et al. (2010) concluded that the focal position of the previous field is a feasible estimate for the subsequent field for well prepared slides.

3.2 Identification of bacilli

Features are attributes, such as colour or length, which would specifically describe an object. In the instance of TB detection, colour, shape, compactness and eccentricity are the most commonly used features (Khutlang et al., 2010a; Veropoulos et al., 1999). These features exploit the unique dimensionality of bacilli and the colour difference between bacilli and the background.

A few research groups have published algorithms on segmentation and classification of TB bacilli in digital images of sputum smears for ZN and for auramine-stained smears (Forero et al., 2006; Khutlang et al., 2010a, b; Sadaphal et al., 2008 and Veropoulos et al., 1999). Pattern recognition techniques were proposed for the first time for the identification of TB in auramine-stained sputum smear images by Veropoulos et al. (1999) and Forero et al. (2001).

Previous researchers Dendere (2009) and Khutlang (2009) have investigated algorithms for the segmentation of objects from ZN-stained sputum smear images. Khutlang (2009) also proposed classification algorithms for the identification of TB bacilli from the segmented objects in ZN-stained sputum smears. Khutlang (2009) segmented and classified images of 100x and 20x magnification obtained from a high-end (Zeiss Axioskop2) microscope. Similarly, Dendere (2009) performed segmentation on 40x and 100x images, also obtained using a Zeiss Axioskop2 microscope.

3.2.1 Sensitivity and specificity

The accuracy of diagnosis is generally expressed in terms of sensitivity and specificity. Sensitivity is the ratio of correct positive decisions against the total number of positive cases and specificity is the ratio of correct negative decisions against the total number of negative cases (Steingart et al., 2006).

$$Sensitivity = \frac{Number\ of\ true\ positives}{Number\ of\ true\ positives + Number\ of\ false\ negatives}$$

$$Specificity = \frac{Number\ of\ true\ negatives}{Number\ of\ true\ negatives + Number\ of\ false\ positives}$$

In other words, sensitivity refers to the probability that a person with TB will test positive and specificity refers to the probability that a person without TB will test

negative. Overall accuracy gives the probability that an individual will be correctly classified by a test.

Evaluating these metrics on a per bacillus basis gives an indication of the accuracy of identifying individual objects in an image correctly as bacilli or non-bacilli. On a per image or per view field basis, one obtains an indication of how accurately an image is identified as containing or not containing bacilli. On a per slide basis, an indication is given of how accurately any slide is correctly identified as containing or not containing bacilli. Per slide sensitivity and specificity values allow comparisons with human operators. In some studies, manual screening of sputum smear microscopy for identifying pulmonary cases is reported to have sensitivity of above 80% whereas in some cases it is in the range of 20-60% (Steingart et al., 2006).

3.2.2 Image segmentation

Image segmentation is the process of partitioning the image into non-intersecting regions so that each region is homogenous and the union of no two adjacent areas is homogenous (Pal and Pal, 1993). In other words, it is the separation of separate entities (objects) in the image from each other and the background. Image segmentation extracts useful information from an image needed for the subsequent steps like feature extraction and image classification. The quality of the final output of pattern recognition depends largely on the segmentation output (Pal and Pal, 1993).

In sputum images, the relationship among the colour components can be taken advantage of to segment the images (Forero et al., 2006). Forero et al. (2006) used a segmentation method based on the combined use of colour information and shape of auramine-stained bacilli. They used Canny edge detection with morphological operators and adaptive colour thresholding for segmentation. This technique extracted most bacilli in auramine-stained sputum images and eliminated most debris. Veropoulos et al. (1999) used the Canny edge detection method for segmenting auramine-stained bacilli from their background. Canny edge detection first smoothes an image to remove noise and then marks the edges where the gradients of the image have high magnitudes. By thresholding the potential edges are determined. The final edges are determined by suppressing the weak edges that are not connected to strong edges.

Sometimes edges of segmented objects are disconnected due to some missing pixels in an image. Veropoulos et al. (1999) applied edge pixel linking to segmented objects to complete broken edge contours. This step links the edges that are disconnected based on an evaluation function representing the validity of edge connectivity (Takahashi K, 2007).

Dendere (2009) explored the use of parametric and geometric deformable models to segment bacilli in images of ZN-sputum smears. Segmentation by a deformable model is a technique that defines a dynamic curve in an image domain and generates internal forces from the curve as well as external forces from image data under which the curve deforms to converge at an object border. To achieve complete automatic segmentation, Dendere (2009) detected objects in an image using Canny edge detection, watershed segmentation and colour segmentation. A deformable model was then initialised around each detected object. Results of his study led to a conclusion that deformable models are able to segment ZN-stained TB bacilli but the long processing time and under-segmentation of bacilli were limiting factors. The shape of bacilli in 40x images was less well retained than in 100x images by parametric and geometric deformable models.

Edge detection and colour gradient-based AFB segmentation perform poorly for ZN-stained images because these images have greater background detail than fluorescent (auramine-stained) images (Sadaphal et al., 2008). Therefore, colour-based Bayesian segmentation was suggested by Sadaphal et al. (2008) to predict the probability of a pixel belonging to a TB bacillus in ZN-stained sputum smears. Their algorithm recognised ZN-stained AFB under varying magnification, staining and resolution, although no accuracies were reported.

There is a significant difference between the RGB (red, green and blue) values of most true AFB pixels and non-TB objects (Sadaphal et al., 2008). Khutlang et al. (2010) used pixel classifiers for the segmentation of ZN-stained bacilli owing to their ability to exploit colour differences between bacilli and background. They evaluated Bayes', quadratic, logistic linear and Euclidean distance linear pixel classifiers (described in Section 3.2.8) for segmentation. Pixel classifiers respond better to the background variability of ZN-stained images than edge detection methods. They are also less likely to miss objects with poorly defined edges.

In Khutlang's (2009) study the Bayes and quadratic classifiers performed the best for segmentation. They both gave the same percentage of correctly classified pixels, 88.39% and of incorrectly classified pixels as 38.08%. The linear classifier produced 87.7% correctly classified pixels and 42.5 % incorrectly classified pixels. The Euclidean distance linear classifier had 85.73% correctly classified pixels and 37.33% incorrectly classified pixels. He then used a product (combination) of three classifiers, Bayes', quadratic and logistic linear for segmentation and 89.38% of correctly classified pixels and 39.52% of incorrectly classified pixels were obtained.

Khutlang (2009) performed contextual pixel classification in conjunction with the Canny edge detector for ZN-TB sputum image segmentation. This gave 93.20% of correctly classified pixels and 50.51% of incorrectly classified pixels on 100x magnification images. It had the highest percentage of correctly classified pixels. However, it also gave a high percentage of incorrectly classified pixels which made it prone to segment non-bacillus objects. The segmentation methods performed poorly on 20x magnification images.

3.2.3 Filtering

Segmented objects are fed to the classifier to determine if they indeed belong to the class of the objects of interest or not. However, before the classification process, several objects can be directly rejected because of their size and/or shape. Forero et al. (2006) filtered the objects according to their size and shape; the objects whose area was too small or too large or whose eccentricity was very low were filtered. Khutlang (2009) and Veropoulos et al. (1999) filtered objects based on size. The filtering process can be optimised by exploring acceptable value ranges of different features. Khutlang (2009) filtered objects of area less than 50 pixels and above 400 pixels from images of 100x magnification.

3.2.4 Segmentation evaluation

Khutlang (2009) used an evaluation procedure based on manually segmented reference images to evaluate Bayes', linear, quadratic and Euclidean distance linear classifiers. He

computed the ratio of correctly classified pixels (common rate) and the number of incorrectly classified pixels with respect to the reference image (difference rate).

Dendere (2009) used the Hausdorff distance (Huttenlocher et al., 1993) for comparing images to validate the segmentation. Manually segmented images served as the gold standard for comparison with algorithm-segmented images. Khutlang et al. (2010) also assessed his selected segmentation method, product of Bayes', quadratic and linear classifiers, using the Hausdorff distance.

The Hausdorff distance measures how far each point of a reference set lies near some point of an image set and vice versa (Huttenlocher et al., 1993). It can be used to determine the degree of similarity between two objects superimposed on one another.

Given two finite point sets $A = \{a_1, a_2, \dots a_p\}$ and $B = \{b_1, b_2, \dots b_q\}$, the Hausdorff distance ($H(A,B)$) can be defined as (Huttenlocher et al., 1993).:

$$H(A,B) = \max\big(h(A,B), h(B,A)\big)$$

where $h(A,B) = max_{a\in A} min_{b\in B} \|a-b\|$ and $h(B,A) = max_{b\in B} min_{a\in A} \|b-a\|$; $h(A,B)$ and $h(B,A)$ directed Hausdorff distance from A to B and B to A respectively. $\|a-b\|$ is a distance metric.

3.2.5 Feature extraction

Features can be extracted from the segmented objects. Features are certain characteristics that describe an object which distinguishes it from other objects. Shape and colour are the important bacillus features. Veropoulos et al. (1999) used shape descriptors that allowed numerical representation of auramine-stained bacilli. Veropoulos et al. (1999) found fifteen Fourier descriptors which were sufficient to represent each object. Forero et al. (2006) evaluated the following features for bacillus characterisation: area, compactness, major and minor axis lengths, eccentricity, perimeter, solidity, Hu's moments and Fourier descriptors. However, scale, translation and rotation invariant features are preferred for the representation of bacilli as they give a more robust identification. Therefore, Forero et al. (2006) chose only compactness, eccentricity, Hu's moments and Fourier descriptors. The features Khutlang (2009) chose were eccentricity, compactness, Fourier descriptors, moment invariants and colour features.

Eccentricity and compactness

The ratio between the foci and the long axis lengths of an object's best fitting ellipse is defined as its eccentricity (Forero et al., 2006).

Compactness is the ratio of perimeter (P) and area (A) of the object, $c = \frac{P^2}{A}$; it measures how close the shape of the object is to a circle (Forero et al., 2006). Therefore, the long and thin characteristics of bacilli may be described by eccentricity and compactness.

Fourier features

Fourier descriptors are used to describe the shape of an object. The shapes are described by first extracting the boundary of the object and then converting it into Fourier descriptors. The boundary can be represented as a complex sequence of coordinates starting at an arbitrary point (Gonzalez et al., 2004):

$$s(k) = x(k) + jy(k)$$

for k = 0,1,2,…$K-1$. K is the number of boundary pixels. In the above equation the second value of each coordinate is made imaginary (for the purpose of determining the Fourier transform). The discrete Fourier transform of $s(k)$ is:

$$a(u) = \sum_{1}^{K-1} s(k) e^{\frac{-j\pi\, 2ku}{K}}$$

$a(u)$ for u = 0,1,2… $K-1$ gives the complex coefficients that can be used as Fourier features (Gonzalez et al., 2004).

The transform $r(u) = \sqrt{|a_{x(U)}|^2 + |a_{y(U)}|^2}$ makes the Fourier features invariant to translation and rotation whereas scale invariance is achieved by the transform, $w(u) = r(u)/r(1)$; $a_{x(U)}$ and $a_{y(U)}$ are the real and imaginary parts of the descriptors (Sonka, 2008). The scale, rotation and translation invariant properties make Fourier features a robust method as the bacilli are often found to lie in different directions and they maintain a rod shape but in variable sizes.

Moment invariants

Moment invariants are contour-based or region-based shape descriptors and are rotation, translation and scale independent. Mindru et al. (2004) investigated moment invariants

that combine shape and colour information to recognise coloured patterns like labels, logos or pictograms. The invariant features that Mindru et al. (2004) validated are functions of generalised colour moments. They are invariant under both geometric deformations and photometric changes and were therefore considered relevant to the description of bacilli. Generalised colour moments combine powers of pixels coordinates and their intensities in the individual colour channels. Thus they characterise the colour and shape distribution of a pattern uniformly. The generalised colour moment is defined by (Mindru et al., 2004):

$$M_{pq}^{abc} = \iint_{\Omega} x^p y^q [R(x,y)]^a [G(x,y)]^b [B(x,y)]^c \, dx \, dy$$

where M_{pq}^{abc} is said to be a generalised colour moment of order $p+q$ and degree $a+b+c$. Generalised colour moments of degree zero are shape moments of an image whereas those of degree one are intensity moments of the RGB channels (Khutlang, 2009). Generalised moments of order zero are the non-central moments of the colour distribution in the image.

A large set of generalised moments can be extracted even for low orders and degrees and this increases the robustness of the invariants.

Colour features

The ZN-stained bacilli are reddish in colour on a blue background. Therefore colour features may be useful to distinguish TB bacilli in ZN-sputum images. Veropoulos (2001) used the mean and standard deviation of RGB values inside and around an object as colour features and Fourier features as shape descriptors for objects in ZN-stained sputum images. Colour features will differ if images are captured under different lighting conditions. Khutlang et al. (2010) used the mean and standard deviation of RGB colour features inside an object and from the centre pixel of the object.

3.2.6 Feature selection

A subset of features may be selected to extract only those features that contribute most to classification. Different selection methods were used by Khutlang (2009) for feature subset selection. He used population-based incremental learning (PBIL), correlation based feature selection (CFS), sequential floating forward selection (SFFS) and branch

and bound (B&B) feature selection methods. The feature subset selected by PBIL obtained the highest classification accuracy.

Khutlang's (2009) PBIL was based on Thornton's separability index (SI). SI is defined as the fraction of a set of data points whose classification labels are the same as those of their nearest neighbours. In PBIL, selection of feature subsets is made probabilistically. Subsets that yield a higher SI evaluation prejudice the progressive search by using weights (Baluja, 1994).

3.2.7 Fisher mapping

The Fisher transform generates a better discrimination between classes by mapping the feature space to a low dimensional space. It is a dimensionality reduction technique (Franco et al., 2006). It is based on the optimisation of the between-class scatter matrix S_B with respect to the within scatter matrix S_W.

S_B defines the between-class distances for all classes:

$$S_B = \sum_{i=1}^{m} P_i(u_i - u_o)(u_i - u_o)^T$$

where u_o is the global mean vector and u_i is the mean of each class i.

S_W defines the variance of features for each class:

$$S_W = \sum_{i=1}^{m} P_i S_i$$

where S_i is the covariance matrix for each of the m classes; P_i is the prior probability of each class.

Linear Fisher mapping finds a linear combination of features which separates two or more objects. The non-linear Fisher transform is generally used for problems with low separability between classes. Khutlang (2009) used linear Fisher mapping since TB identification is a two-class problem. He found that all classifiers performed better with sensitivity and specificity above 95%, when Fisher mapping was applied to the feature set.

3.2.8 Classification

A classifier predicts the class of an object. It is the final step in an identification process. There are two types of classifiers, supervised and unsupervised. A supervised classifier maps objects to labels by learning from labeled example objects. An unsupervised classifier does the same by learning from example objects with no labels; clustering is first performed to learn intrinsic classes in the training data. Generalisation performance is the discriminative power of a classifier to draw the decision boundary between two classes (Duda et al., 2001). Good generalisation performance is obtained from a classifier with optimal complexity, i.e. if a classifier is more complex than the optimum required, the boundary is prone to noise and over-fits training data and vice versa (Khutlang, 2009).

Segmented objects may be presented to a classifier for its class to be determined. To be able to identify the class of an object from the features presented to it after the feature extraction stage, a classifier should be trained beforehand with the feature information of the entity to be classified (Friedman and Kandel, 2000). A training set contains extracted features of manually labeled objects and corresponding labels. An unseen data set (test set) is given to the trained classifier algorithm to test if it correctly classifies the objects.

In automated TB microscopy, features extracted from segmented objects are fed in to a classifier to determine whether or not these objects are bacilli. Veropoulos et al. (1999) used techniques based on artificial neural networks for the detection of bacilli in auramine-stained sputum smears. They achieved sensitivity of 94.1% and specificity of 97.67% for the detection of individual bacilli in captured auramine-stained sputum images and concluded that an automated method is practicable. Forero et al. (2006) attained a sensitivity of 97.89% and specificity of 94.67% per image. See Table 2 for the results obtained by various researchers. Khutlang (2009) used object classifiers: logistic linear, Bayes', quadratic, kNN, SVM and PNN for classification. The accuracy he obtained for these classifiers is given in Table 3. kNN gave the highest accuracy whereas quadratic, linear and Bayes' classifiers gave the highest sensitivity.

Khutlang (2009) performed classification on 100x images using two-class and one-class classification and on 20x images using two-class classification. He found that two-class classifiers performed better than one-class classifiers. He achieved a specificity and

sensitivity of above 95% per bacillus, using two-class classification on both 100x and 20x ZN-images. For one-class classification on 100x ZN-images, a sensitivity and specificity of above 90% was achieved.

Table 2: Sensitivity and specificity results obtained in previous related research

Study	Type of image	Sensitivity (%)	Specificity (%)
Khutlang (2009), two-class	ZN, 100x & 20x magnification	>95%	>95%
Khutlang (2009) one-class	ZN, 100x magnification	>90%	>90%
Veropoulos (1999)	Auramine, 40x magnification	94.1%	97.67%
Forero et al. (2006)	Auramine, 25x magnification	97.89%	94.67%

Table 3: Accuracy obtained for various classifiers in Khutlang's (2009) study

	Classifiers					
	kNN	**Bayes'**	**Linear**	**Quadratic**	**PNN**	**SVM**
Accuracy (%)	88.9628	68.2423	83.2263	76.9619	85.0161	79.3254
Sensitivity (%)	99.1295	99.6736	99.8912	100	99.5103	99.1295
Specificity (%)	81.5476	45.3175	71.0714	60.1587	74.4444	64.8810

PNN and SVM classifiers

PNNs (probabilistic neural networks) are radial basis function (RBF) networks that replace each data point by a kernel. The probability density functions (PDF) of the training data are estimated from these kernels. The class whose PDF dominates at the position of a query object is estimated and its label is assumed by the query object (Khutlang, 2009).

Support vector machines map the given dataset into a high-dimensional feature space. They then try to locate in that space a plane that separates the two classes.

Bayes' classifier

Bayesian decision theory (Duda et al., 2001) forms the basis of Bayes' classifier:

$$P(A|x) = P(x|A) * \frac{p(A)}{p(x)}$$

where $P(A|x)$ is the probability that an instance x belongs to class A, $p(A)$ is the prior probability, $P(x|A)$ is the likelihood of x if A is true and $p(x)$ is the normalisation constant. The equation calculates the probability that A would occur providing that x has happened. It assumes that the decision problem is expressed in probabilistic terms and therefore is a supervised statistical approach to pattern classification (Meurie et al., 2003). An object is assigned a class that has the highest $P(A|x)$. The probability of error in assigning a class to an object is minimised by Bayes' classifier. Bayesian classification for the identification of bacilli and non-bacilli in images of auramine-stained smears was used by Forero et al. (2006).

Linear classifier

The linear regression classifier establishes a linear mapping between stored points and their labels. The mapping is used to predict labels of query points. The error between classes in the least square sense is minimised by the mapping using the Euclidean distance. The logistic linear classifier is attained by iteratively reweighting the least squares solution to the plot of a line separating the two classes (Fukunaga, 1990).

Quadratic discriminant classifier

A quadratic mapping is established between objects and their labels using the information like mean and covariance estimated from the training data points. The quadratic classifier presumes the classes of the dataset to have normal density functions. It is a density based classifier which uses covariance matrix and mean vector to estimate the density distribution for each class. The quadratic function (Fukunaga, 1990):

$$\frac{1}{2}\left(\left(X - M_1\right)^T \sum\nolimits_1^{-1} \left(X - M_1\right)\right) - \frac{1}{2}\left(\left(X - M_2\right)^T \sum\nolimits_2^{-1} \left(X - M_2\right)\right) + \frac{1}{2} ln \frac{|\sum_1|}{|\sum_2|} >/< ln \frac{P_1}{P_2}$$

where X is an object feature vector M is the mean vector, Σ is the covariance matrix and P_1 and P_2 are prior probabilities of the classes.

The class mean and covariance matrices are used to draw the discrimination between classes. The quadratic classifier labels objects based on their inequality (Fukunaga, 1990).

Nearest neighbour classifier

The nearest neighbour classifier compares the Euclidean distance between each query point and the stored objects to predict the labels of the query points. The query point gets assigned the label of the stored point that has the lowest Euclidean distance. When k points are compared, the NN becomes kNN classifier. Then the query point is assigned the label of the majority of its classifiers.

3.2.9 Cross-validation

Cross validation is used to evaluate learning algorithms by dividing data into a training set and test set (Duda et al., 2001). A classifier would use the training set to learn a model and the test set to validate the classifier performance. For example, a dataset containing 100 objects can be divided into 10 subsets where one subset is used for training and tested on another. The test set is then added on to the training set and the new training set can be validated on another testing set. When this is done 10 times, it is called 10-fold cross-validation. In general, k-fold cross-validation may be used to evaluate the classifier. The average of the validation results are taken at the end.

4. Materials and Tools

The materials and tools used in this study mainly consist of a microscope hardware platform and ZN- stained sputum slides.

4.1 ZN-stained sputum slides

The ZN stained sputum smear slides for this investigation were prepared by the South African National Health Laboratory Services (NHLS) at Groote Schuur Hospital in Cape Town. Positive and negative slides were obtained. All the positive slides were confirmed positive and their grading (refer to Table 1) was provided by the NHLS. A total of 250 slides were procured from the NHLS. Among these only 132 slides were of good quality (without much stain or smear inconsistency) out of which 70 were TB negative and 62 were TB positive slides.

4.2 40x images

Images of the above mentioned ZN- slides, taken at 40x magnification as shown in Figure 7, comprised the data for the study. The images were of 1392 x 1040 pixels resolution.

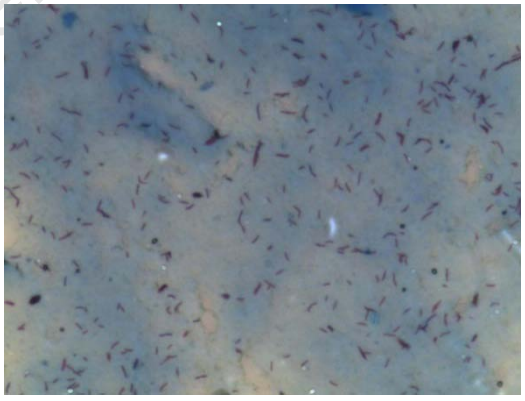

Figure 7: A typical image produced by the Nikon microscope at 40x magnification

4.3 Hardware Platform

An automated stage, a digital camera and a commercial microscope comprised the hardware platform (Figure 8), which was built outside of the project, is described here. An illustration of the hardware platform is shown in Figure 9.

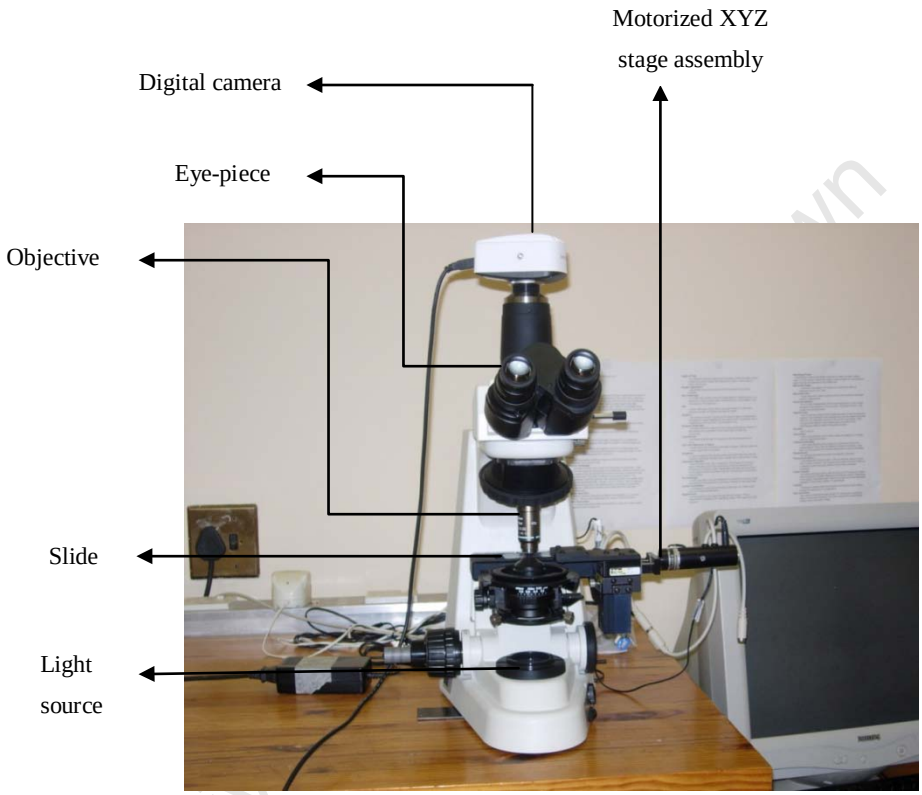

Figure 8: The hardware platform used in this study

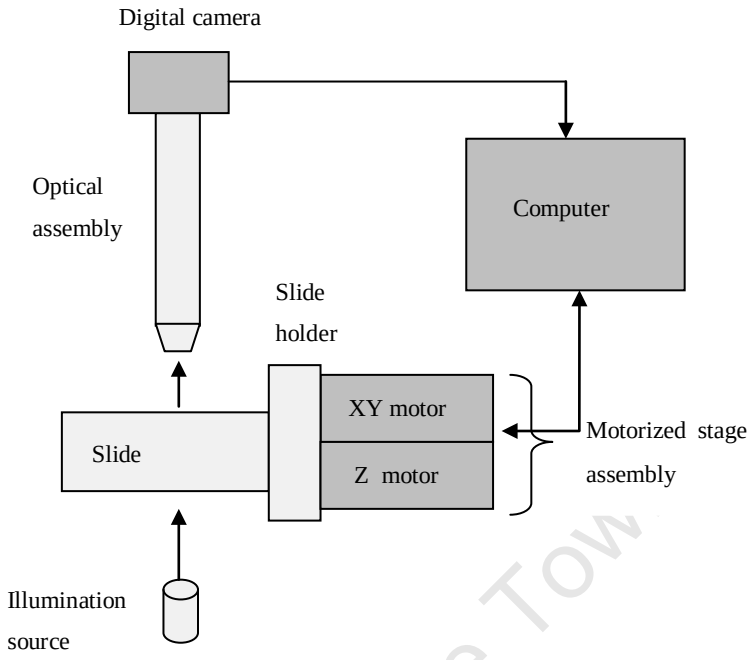

Figure 9: Illustration of the hardware used in this study

4.3.1 Microscope and slide holder system

The hardware platform was built around a Nikon eclipse 55i microscope with a 40x/0.65 NA aperture. A custom-made stage replaces its original stage. This stage has a simple slide holder. It is a cantilever slide holder system as shown in Figure 10 where one end of the slide can be inserted into the holder. This stage design was incorporated to make the system cost-effective. The drawback of this system is that slides that are thicker than 1mm cannot be inserted into the holder.

An oil-immersion objective is used to obtain 100x magnification whereas for 40x (lower power) magnification a dry objective is used. A dry objective avoids the need for oil as the medium between a slide and the objective lens. Moreover, the same area of a slide can be assessed in less time when using 40x magnification objective compared to 100x magnification objective. Therefore the hardware used in this study comprises of a 40x magnification objective.

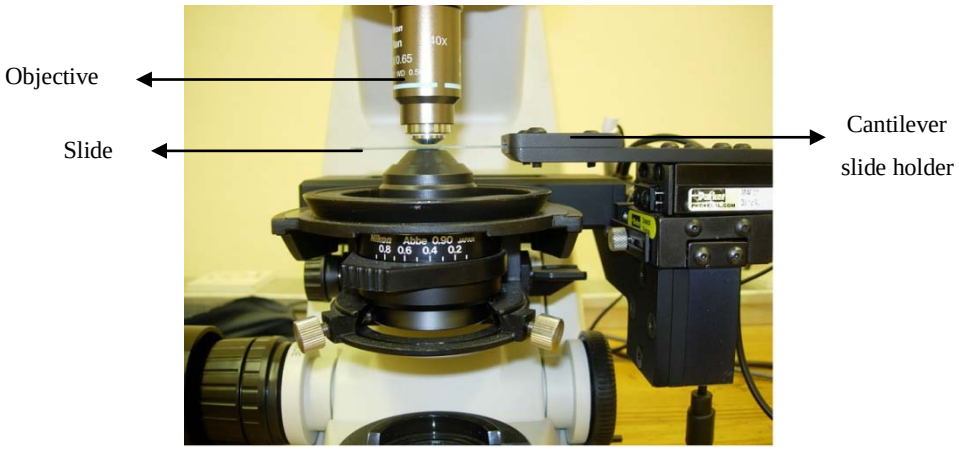

Figure 10: Image of the cantilever slide holder system in the hardware

4.3.2 Motorized stage

In this project the aim was to make the automated TB detection microscopy system as economical as possible and hence a low-end low-cost stage controlled by a stepper motor was used. Commercially available motorized stages are very expensive and therefore a customised stage was built. Commercially available stages are more stable, and have similar but much smaller stepper motors integrated into the stage – hence the higher cost. In the adapted Nikon system, two Zaber T-LA28 linear actuators with integrated stepper motors and controllers for the x- y- movement are installed. These devices turn by a step (constant angle) for every electrical impulse sent to them allowing the system to be built without feedback, reducing total system cost (Zaber, 2011). A software package allows automatic control of stage movement from the computer.

4.3.3 Focus motor

The focus drive (z-axis) uses a stepper motor from Tofra (Tofra, 2010) for high resolution movement of the fine focus and at the same time retaining manual movement of the coarse focus. It uses a high torsion stiffness flexible coupling and requires no modification of the microscope for its mounting. This results in easy installation and low cost. Software provided by Tofra controls the focus drive from the computer.

4.3.4 Digital camera

A Lumenera, Infinity 2-1C 1.4 mega-pixel digital camera is attached to the microscope to capture images of the fields viewed in sputum slides. This camera has a Sony ICX205 sensor of pixel size 4.65µm (Lumenera). Image capture was facilitated using the code supplied with the Lumenera camera. The resolution of images used was 1392 x 1040 pixels with an average size of 80kb.

This camera has a feature called the crop factor which is relevant for this project. When the entire field of view of an objective lens is not captured by the camera sensor, the image is said to be cropped. This is illustrated in Figure 11. When the cropped image is displayed on a monitor, it results in an apparent greater magnification than the magnification contributed by the lens.

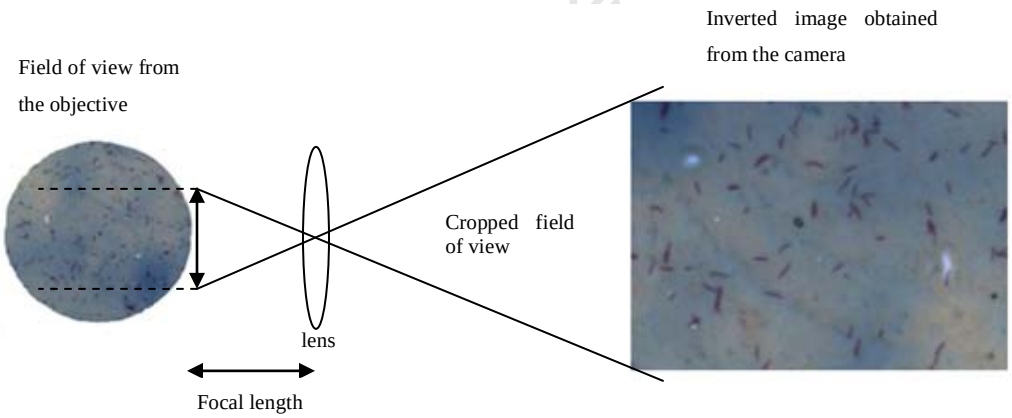

Figure 11: Illustration of crop factor based on a ZN-TB field

4.3.5 Processor

Control and storage of data are effected through a processor/computer connected to the microscope. The work was implemented on MATLAB 7.3.0 (2006b) which runs on a Pentium 4 computer with 1GB RAM.

4.3.6 Stage micrometer

A stage micrometer is a microscope slide used for linear measurement of the specimen being observed, with a finely divided scale marked on its surface as shown in Figure 12. It is a millimetre ruler that is subdivided into increments of 10 and 100 micrometers (Nikon MicroscopyU, 2010). The micrometer is used in this study for various hardware testing methods.

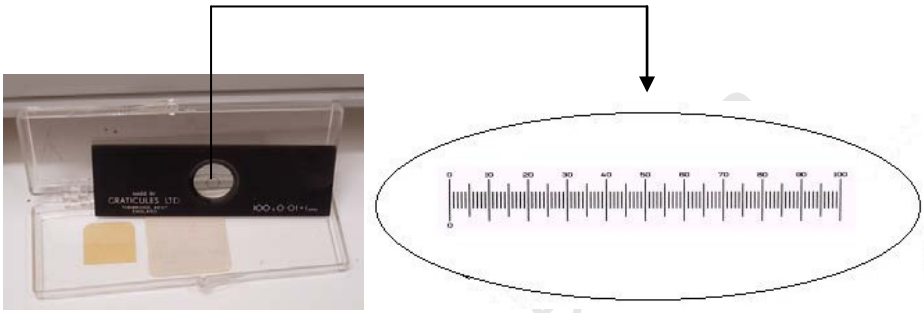

Figure 12: A micrometer slide

4.4 Software

The algorithms developed by previous researchers, i.e. the segmentation and classification algorithms developed by Khutlang (2009) and the auto-focusing algorithms developed by Osibote et al. (2010) are used. All the programs are written in MATLAB.

5. Methods – Auto-focusing, Segmentation and Classification

This chapter details the methods that were used for the automated identification of bacilli. Auto-focusing, image segmentation and classification methods are described here.

Most of the methods were based on the research on best performing methods proposed by researchers whose work was closely linked to the same application.

Auto-focusing was performed to produce an in-focused image of the field of view. Pattern recognition was performed on the focused image for the identification of bacilli. Segmentation and filtering were used to extract candidate objects from the focused image. Selected features that were significant for the determination of the class of the object were normalised, mapped using Fisher transform and presented to the classifier, which produced labels indicating if objects were bacilli. An overview of these steps is given in the Figure 13.

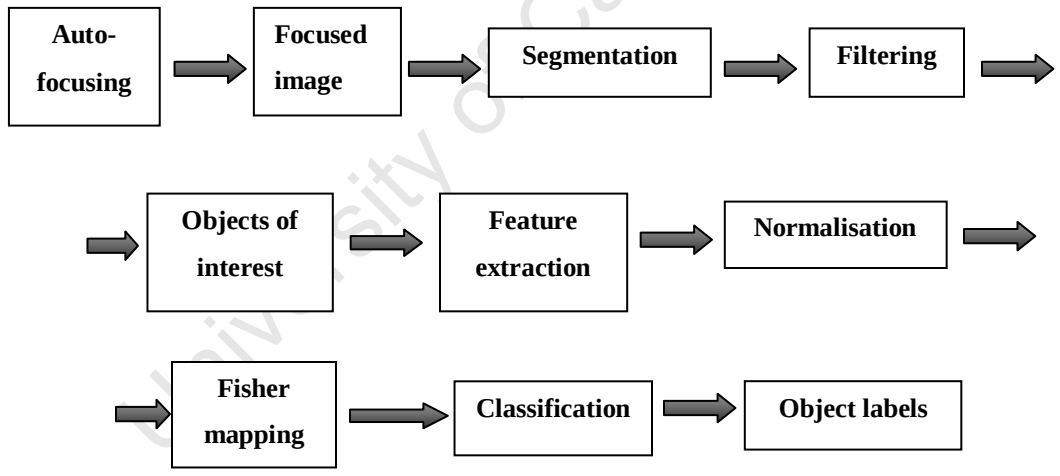

Figure 13: An overview of the steps followed for bacilli identification

5.1 Auto-focusing

Subsequent image analysis steps depend on auto-focus; a better focused image yields better segmentation and classification results. The method followed to achieve auto-focus in this study is discussed here.

5.1.1 Focus measure

The requirement for calibration and look-up tables is a limitation for active auto-focusing, and published auto-focusing solutions primarily rely on passive focusing. Comparison and selection of focus measure and search algorithm methods for passive auto-focusing was done by previous researchers (Osibote et al., 2010) for the same application of TB detection. Although it can be computationally expensive, passive auto-focusing is flexible, more accurate and easy to implement (Mea et al., 2005) and the results of the comparative study done by Osibote et al. (2010) were implemented in this project. Vollath's F_4 focus measure proposed by Osibote et al., (2010) was selected for implementation.

5.1.2 Finding the optimal focus position

Initial focusing (for the first field) required acquisition of several images along the optical axis to extract information to calculate the position at which the best focused image would lie. The step size was determined using the calculation given in Section 3.1.4 using parameters for the imaging system used in this project: λ=500nm; η=1; NA=0.65; M=40. Therefore 1.2µm is the minimum but optimum distance to capture images along the z-axis and was fixed as the step size throughout the study. The global search method implemented scans *n* lens positions (*n* is the number of images to take in the first stack of the first field in a slide) at fixed intervals of 1.2µm for the first field in a slide and computes the associated focus function. The possibility of the position of optimum focus lying between the fixed positions at which the images are captured motivated Osibote et al. (2010) to use a fast Fourier transform-based interpolation based method to interpolate the focus function between the image positions. The algorithm then sends the lens to the position with the highest focus measure on the curve. A similar approach was used in this study.

Automated TB detection requires a number of fields to be scanned. The curve fitting approach of Yazdanfar et al. (2008) used by Osibote et al. (2010) was used in this study. This method reduces the time consumption due to multiple stage movements through different z-axis positions by using only three images per field. For successful application

of the curve fitting technique, images used to fit a curve have to be captured around the true focal position, in this regard, the focal position obtained from the previous field serves as an estimate focal position for the subsequent field. Curve fitting was not applied for the first field but the position of the best focused image i.e. the image with the highest focus measure in the stack was chosen.

5.1.3 Automated movement of the stage to the position of maximum focus

The movement of the z-axis stage was facilitated from MATLAB. There was no position feedback with respect to reference positions from the motor. This impeded the positioning of the stage at any desired position. This problem was resolved by using the starting position with respect to the objective as the reference (zero position) and keeping track of the steps moved in any direction during any stage movement in the entire process of analysing a slide. Depending on the direction, steps were incremented and decremented to the distance already travelled from the reference position so that the reference position is always zero.

5.1.4 Auto-focusing on adjacent fields

In an ideal slide, focus levels of adjacent fields are expected to be close. However, the extent of the difference in focus levels between adjacent fields may vary according to slide quality and the use of curve fitting may produce poor images in slides with high variation. For this reason, a threshold was set to determine the suitability of curve fitting between fields. If the difference between the focal positions of the previous field and current field that has currently been found using curve fitting is greater than 1.2 um then the position determined by curve fitting is not applied but a full stack is used and the focal position is re-calculated instead.

Once a focused image of a field is captured the next step is to segment the image to find objects in the field and then classify those objects to identify if they are bacilli or not. The segmentation and classification methods applied in this study are described below.

The auto-focusing method proposed by Osibote et al. (2010) was implemented during system integration and its performance is evaluated during the system evaluation. Therefore the auto-focusing methods used were not individually evaluated as Osibote et

al. (2010) had already performed the evaluation of the auto-focusing component separately on images obtained from the same hardware and found it a feasible method for implementation on the microscope prototype.

5.2 Segmentation

Pixel classifiers were considered for segmentation because of the distinguishable RGB values of pixels that contain ZN-stained bacilli. The results Khutlang (2009) obtained for the combination of the three classifiers was similar to the results he obtained from the Bayes and quadratic classifiers. Although the combination of three classifiers produced a small percentage of increase in correctly classified pixels, it also produced a higher percentage of incorrectly classified pixels. Therefore more non-bacillus objects may be presented to the classifier, which in turn may increase the overall processing time. Moreover, the computational cost of combining three classifiers may be eliminated if a single classifier is used.

Bayes', quadratic and linear classifiers were evaluated in this study for comparison, in order to find the better performing classifier to segment ZN-stained sputum images of 40x magnification. These classifiers were compared, as different classifiers may perform differently on images obtained using different hardware platforms.

5.2.1 Training the classifier for segmentation

Areas containing pixels belonging to bacilli and non-bacilli were labelled to train the pixel classifiers for segmentation. Image pixels were used as objects. Labeling was done under the guidance of TB microscopy research group members and pathologists from the South African National Health Laboratory Services at Groote Schuur hospital.

Objects in the images were manually outlined and labeled with the help of a graphical user interface (GUI) available for the research group. Each pixel was assigned +1 or -1 based on whether it belonged to bacillus or not. Bacilli were regarded as positive, while background, stain lumps and debris were considered as negative objects. ZN-images have the distinctive feature of reddish pink coloured bacilli against a blue and sometimes white background. Only bacilli with their length in the focal plane were considered as

positive objects. Ideally, all pixels of reddish pink colour belonging to a bacillus in the focal plane should be picked up by the segmentation method.

5.2.2 Segmentation evaluation after training

The performance of the Bayes, quadratic and logistic linear pixel classifiers was compared visually and using the Hausdorff distance. Manually segmented objects were used as the gold standard. The boundary pixels specified by the gold standard (A), and the set of boundary pixels determined by the segmentation technique (B), were superimposed on one another. The Hausdorff distance was used to evaluate the segmentation results by determining the degree of similarity between A and B.

5.2.3 Filtering

The segmented objects obtained from the pixel classifiers were filtered based on the area of the objects. Objects either too small or too big to be an individual bacillus were filtered out. The threshold for area was determined empirically. This retained mostly relevant objects in the filtered images.

5.2.4 Feature extraction and selection

The best feature subset that differentiates bacillus objects from non-bacillus objects determined by PBIL in Khutlang's (2009) study was extracted from objects that remained after filtering. Features of compactness, eccentricity, Fourier descriptors, moment invariants and colour were used for the identification of bacillus objects.

5.2.5 Normalisation and linear Fisher transform

The selected set of features was normalised so that all features were treated equally to eliminate bias towards the identification of objects and also to minimise the effect of outliers during classification. The absolute difference of each feature and its mean was divided by the standard deviation of that feature to normalise that feature. Linear Fisher mapping was applied on the features for better discrimination of bacilli and non-bacilli. The dataset of features was fed into the classifier for determining the class of the objects.

5.3 Classification

The kNN classifier, which gave the highest accuracy among all the classifiers in Khutlang's (2009) study, was compared with Bayes', quadratic and linear classifiers (these classifiers were also evaluated for the segmentation step) as they gave the highest sensitivity in his study. The classifiers were trained to recognise the class of the segmented objects. A set of images was labeled for training the selected classifiers.

A GUI was developed programmatically for labeling and extracting the labels of corresponding segmented objects in images. A GUI is a pictorial interface to a program which allows communication between user and the machine. The GUI allowed the user to label the segmented objects as bacilli or non-bacilli in the original image. Features associated with the labeled objects were extracted in order to train a classifier for classification.

The Bayes, quadratic, linear and kNN classifiers were trained using the objects labeled as bacilli or non-bacilli (training set) to classify segmented objects. For comparison, the classifiers were evaluated on test data (unseen bacillus and non-bacillus objects). The best performing classifier was combined with the auto-focusing and segmentation software and integrated with the stage movement, image capturing components to work as a unit for automated TB diagnosis in 40x magnification ZN-stained sputum images.

6. Results: Segmentation and Classification

This chapter presents the results obtained for segmentation and classification on 40x images. The suggested methods, according to the results obtained in this chapter, are used for integration.

6.1 Segmentation

The dataset for training the pixel classifiers for segmentation was composed of 92,550 labeled pixels from 70 images. The dataset contained 58,164 pixels belonging to the non-bacillus class and 34,386 belonging to the bacillus class.

Bayes', logistic linear and quadratic pixel classifiers were tested for visual comparison on 273 images: 200 positive and 73 negative images. Preliminary evaluation by visual inspection on smaller training sets was done to refine the number and type of non-bacillus objects included in the training set. Visually, the quadratic classifier performed better than the rest. The segmentation algorithms were validated and compared using the Hausdorff distance. A set of six images was used for the evaluation. Twenty five bacilli from these images were manually outlined to serve as the gold standard. The mean and standard deviation (SD) of the Hausdorff distance between the contours of the gold standard and the segmented objects are given in Table 4. The distance is given in pixels. Examples of manual and algorithm segmentation results are shown in Figure 14.

Figure 14: Examples of manual (black) and algorithm segmentation (red) results overlaid to find the associated Hausdorff distance

Table 4: Performance evaluation of the segmentation methods

	Bayes'	Quadratic	Linear
Mean(SD)	5.69(±1.36)	5.69(±1.36)	6.27(±1.86)

The quadratic classifier was used for segmentation in this study although Bayes' classifier may also be used as both produced similar results. An example of the segmentation results obtained by the different pixel classifiers is given in Figure 15.

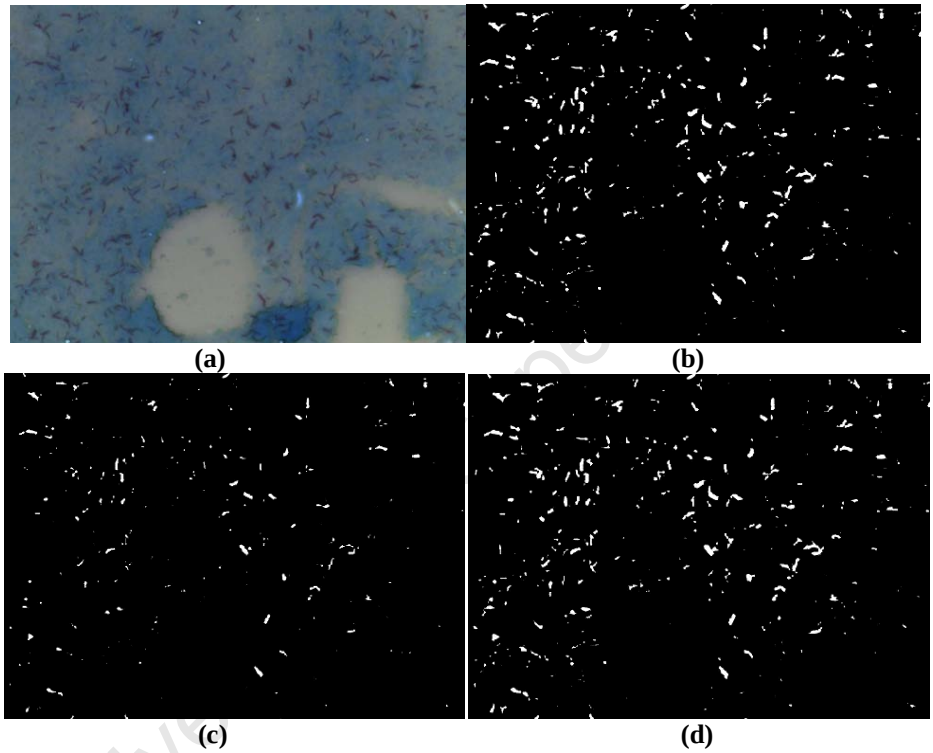

Figure 15: **The original image and the segmented images obtained from different pixel classifiers (before filtering) - a) original image; b) segmented output by Bayes' classifier; c) segmented output by Linear' classifier; d) segmented output by quadratic classifier**

6.1.1 Filtering

The filtering threshold empirically found, removed all connected components/objects with an area of less than 70 pixels and more than 600 pixels. Figure 16 shows the noise reduction as a result of filtering.

(a) **(b)** **(c)**

Figure 16: Results of filtering: a) original image; b) segmented image; c) filtered image

6.1.2 Feature selection

The sixteen relevant features that Khutlang (2009) proposed were extracted from each segmented object. The features were normalised, and mapped using Fisher linear mapping.

6.2 Graphical User Interface

The features used in the GUI are given in Table 5.

Table 5: The GUI features implemented and their associated functions

Main features in the GUI	GUI component	Function
File \ Load	Menu option. Load is a sub-menu item of File menu	Load the original and segmented image from its location as shown in Figure 17.
Overlay	Check box	Overlays the segmented and original images
Select object type	Pop-up menu	Has two options: bacilli and non-bacilli. Select one for labelling the same
Image display	Axis	Displays the image and allows labelling of the segmented objects
Export bacilli	Push button	Assigns +1 label to the corresponding objects labelled as bacilli
Export non-bacilli	Push button	Assigns -1 label to the corresponding objects labelled as non-bacilli
Export label	Push button	All labels of the corresponding objects are written into an Excel sheet

The original image and the segmented image can be loaded into the GUI using the load option in the file menu as shown in Figure 17. Figure 18 shows the loaded image on the GUI screen. The original and segmented images can be overlaid so that the segmented objects may be visible on the original image. The segmented objects are highlighted in yellow. The bacilli and non-bacilli options in the pop-up menu allow the user to label the objects of preference (for example, well defined individual bacilli instead of clumps of bacilli) as bacilli or non-bacilli (see Figure 19). All the labeled bacillus objects are given the label '1' and non-bacillus objects '-1'. The objects that have already been labeled are no longer highlighted in yellow to prevent the user from re-labeling the objects. At the end of labeling, the labels of all the segmented objects are stored in an Excel sheet. The objects that were not selected at all are eliminated so that only the selected objects remain.

Different functions are performed by the push buttons on the right side of the GUI: export bacilli to congregate all the bacilli labels, export non-bacilli to congregate all the non-bacilli labels and export labels to concatenate bacilli and non-bacilli labels together into an Excel sheet.

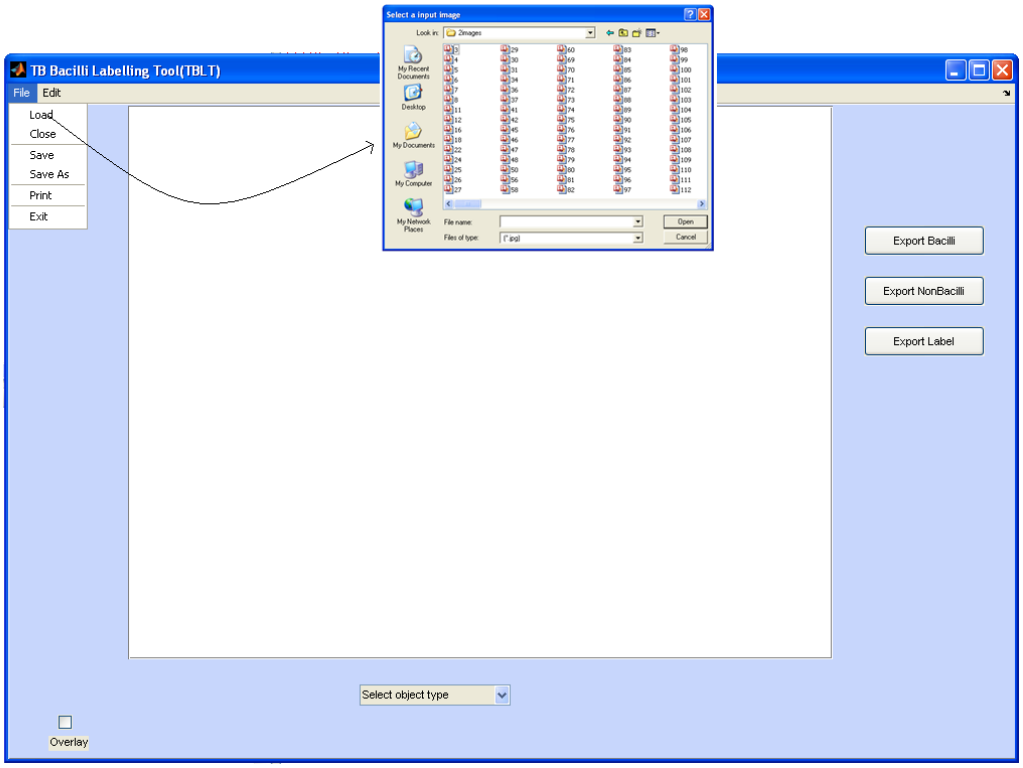

Figure 17: A Screen shot of the GUI: loading an image from a folder on to the GUI

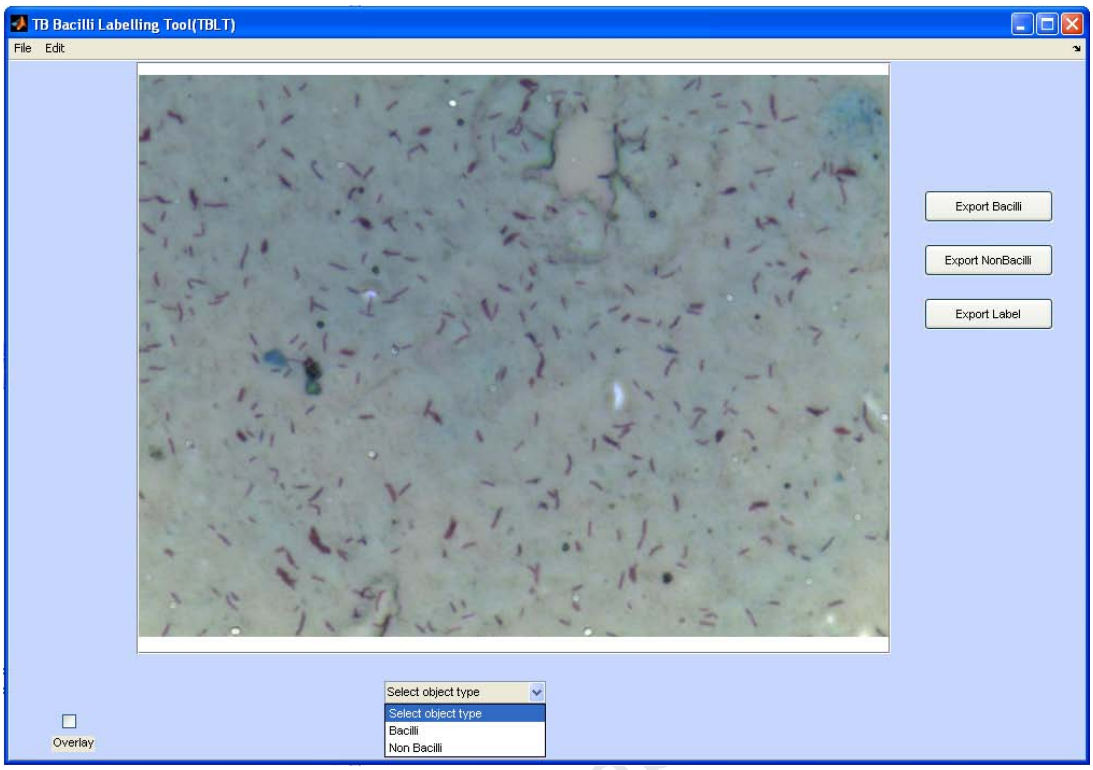

Figure 18: Loaded original image displayed on the GUI: options to label bacilli and non-bacilli in the pop-up menu are illustrated

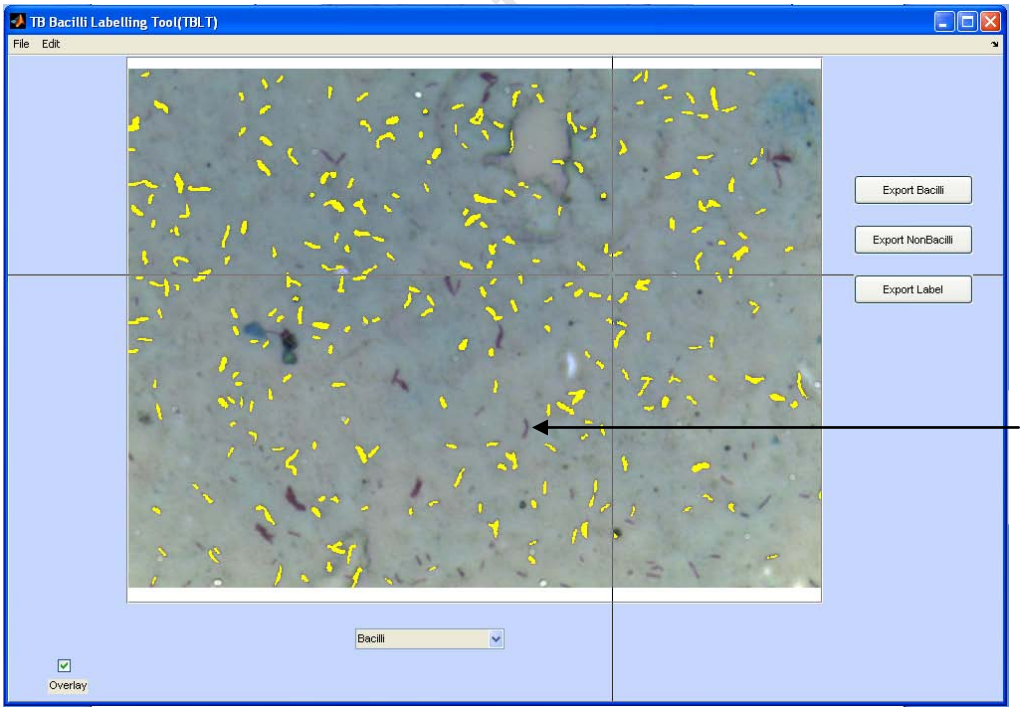

Figure 19: A Screen shot of the GUI while labeling the segmented objects overlaid on the original image as bacilli or non-bacilli

6.3 Classification

A dataset of 3181 objects from 83 images was used for training the classifiers considered for the identification of bacilli in ZN-stained sputum images. From the dataset 1636 objects were bacilli. The kNN, linear, quadratic and Bayes' classifiers were tested on a different test dataset of 1384 objects obtained from 25 images. The results are shown in Table 6.

Table 6: Performance evaluation of classifiers in identifying bacilli in ZN-sputum smears

Classifier	Sensitivity (%)	Specificity (%)	Accuracy (%)
Linear	95.72	90.49	91.60
Bayes'	89.31	96.4	94.89
Quadratic	87.2	96.4	94.44
kNN	92.51	96.11	95.35

The kNN classifier gave the best accuracy with good sensitivity and specificity. Therefore, kNN was selected to identify bacilli in 40x magnification images of ZN-stained sputum obtained from the hardware system. The kNN classifier was further evaluated to check if it gave comparable results to that of other related research given in the literature review.

Further evaluation of the kNN classifier

The kNN classifier was further trained using a larger dataset of 13,934 objects from 255 images. This was inclusive of the dataset used for the determination of the best classifier for this application. Among those objects 9,421 objects were bacilli. Two examples of images classified by the kNN classifier to identify bacillus objects are shown in Figure 20 and Figure 21. The evaluation of the kNN classifier is given below.

(a) **(b)** **(c)**

Figure 20: Example 1: a) original image; b) segmented image; c) bacilli identified by the kNN classifier are highlighted in red

(a) **(b)** **(c)**

Figure 21: Example 2: a) original image; b) segmented image; c) bacilli identified by the kNN classifier are highlighted in red

On a per bacillus basis

k-fold cross validation was used in this step to evaluate the kNN classifier. The dataset was divided into 9 folds. The average of the results obtained is given in Table 7.

Table 7: Evaluation of the kNN classifier on a per bacillus basis

Sensitivity (%)	Specificity (%)	Accuracy (%)
98.31	94.52	97.05

On a per field/image basis

Evaluation of the kNN classifier on a per image basis was performed on a new set of 450 positive images and 650 negative images obtained from a new set of slides. An image was considered positive if at least one bacillus was detected in it. The results are given in Table 8.

Table 8: Evaluation of the kNN classifier on a per field/image basis

Sensitivity(%)	Specificity(%)	Accuracy (%)
97.5	96.62	97

On a per slide basis

Evaluation of the kNN classifier on a per slide basis required the system to be completely automated and integrated with the selected methods. Therefore, the results are obtained while evaluating the full automated system in Section 9.2.

6.4 Discussion

The segmentation algorithm gave good results by picking up most of the reddish pink pixels belonging to bacilli. However, some of the slides had stains that did not have good contrast because of fading or improper staining. This made the bacilli appear either faint or too dark (almost purple) and affected the performance of the segmentation algorithm.

A large number of non-bacillus objects were segmented during the preliminary evaluation of the segmentation algorithm due to the large amount of artefacts like debris, brown stains, and contours of non-bacillus regions incorrectly picked up by the pixel classifier. It was observed that some of the brown contours incorrectly picked up had a pinkish, purplish tint when viewed under large magnification as shown in Figure 22. These objects were segmented as their colour overlapped with that of bacilli. Therefore, the training set for segmentation included a higher number of non-bacillus objects. This effectively reduced the number of objects incorrectly segmented.

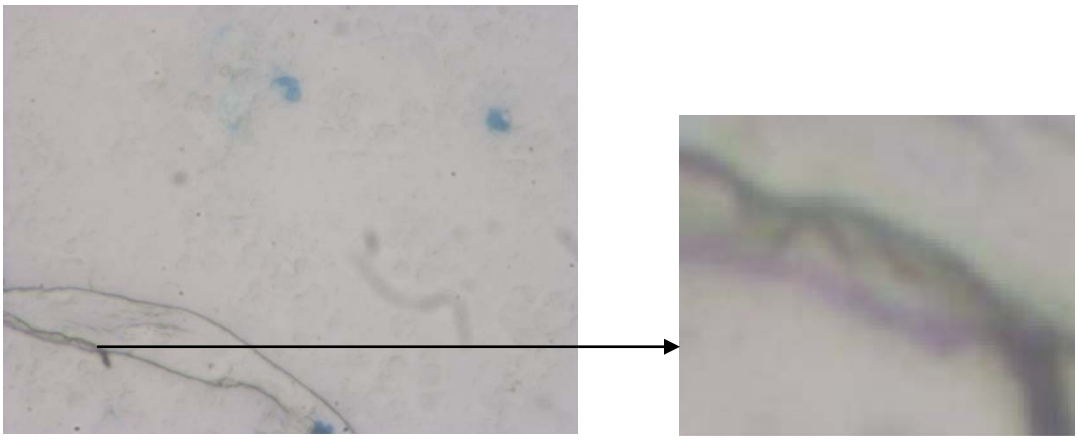

Figure 22: An example of brown contour with purplish tint that segmentation tends to incorrectly pick up

Segmentation was evaluated using the Hausdorff distance and obtained a mean of 5.69 and standard deviation of 1.36 for the quadratic pixel classifier which is a better result than that obtained by Dendere (2009) using active contours, and comparable to that of Khutlang et al. (2010). By visual inspection most of the segmented bacillus objects by quadratic classifier had satisfactory shape. Therefore, the quadratic classifier was deemed a feasible segmentation method to use with the images obtained from the adapted Nikon microscope.

Filtering effectively retained only the relevant information in the images. The threshold area that effectively reduced noise in images of 40x magnification in this study is close to the threshold area used by Khutlang (2009) for 100x images. One would however expect the threshold area to be smaller for a less magnified object. This result may be due to differences in the crop factor and camera resolution (Section 4.3.4) between the cameras used.

The fields containing many bacilli (3+ samples) gave almost 100% sensitivity on a per image basis test. It was observed that some of the sparse fields were resulted as false negatives. This may be because of the inclusion of some of the above mentioned non-bacillus objects in the segmentation training set (having brown contours with purple tint) to reduce false positives. Some bacillus objects with purplish tint may have been classified as negative. Ideally, bacilli should be reddish pink in colour when stained properly. Performance was good on fields with a good blue background and reddish pink

bacilli. Further improvements may be possible by more careful selection of objects for segmentation training.

Forero et al. (2006) performed the test on 473 negative and 169 positive images and obtained sensitivity of 94.67±3.39% and specificity of 97.89±1.3%. Khutlang (2009) achieved the highest accuracy and sensitivity rate of 98.6% and 97.8% and a specificity of 99.12% for the kNN classifier. In this study, the kNN classifier produced a sensitivity of 97.5% and a specificity of 96.62%.

Although the images obtained from the microscope-camera system in this study did not produce as high a quality image as Khutlang's (2009), the trained classifiers still produced a comparable result to that of Khutlang's study. Examples of images used in Khutlang's study and in this study are shown in Figure 23. At 20x magnification the ability of the segmentation algorithm to distinguish the red colour of bacillus objects was affected by the focus of the microscope (Khutlang, 2009). Therefore, 20x magnification was not considered in this study as it did not give satisfactory segmentation results in Khutlang's study. The algorithms performed well on 40x magnification images and therefore are suitable for the identification of bacilli in ZN-sputum images of both 100x and 40x magnification when well trained by a variable training set.

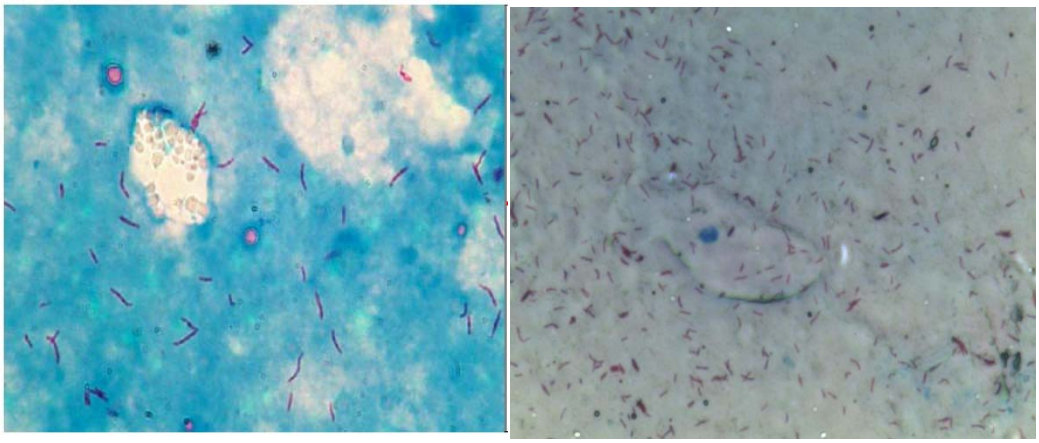

(a) **(b)**

Figure 23: a) An example of a focused 100x image obtained from a microscope-camera system used in Khutlang's (2009) study; b) An example of a focused 40x image obtained from the hardware used in this study

7. Hardware Testing – Methods and Results

This chapter explains the hardware tests that provided useful information for the integration of the system. The methods and results of each section are presented together since some subsequent tests relied on the results of earlier tests.

7.1 Introduction

Tests were conducted to determine the characteristics of the hardware that may help improve the software implementation. Some tests were carried out on the hardware to determine the stability of the system before implementing any software while others were conducted during the implementation of selected software. Therefore the hardware testing and the integration described in the next chapter are inter-connected.

7.2 Preliminary tests

The tests mentioned in this section were conducted during the initial stages of the project to study the stability of the x-, y- and z- axes motor movements before the integration of the selected algorithms with the hardware.

7.2.1 Accuracy of x- and y-axis movement

Methods

The accuracy of the stage movement along the x- and y-axis was tested following a similar method to that suggested by McKeogh et al. (1995) and described in Section 2.7 This test gave an insight as to the stability of the x- and y-axis motor movement. It shows if there is any large variability in positioning when moving the stage and then bringing it back to the original position.

A micrometer slide (Section 4.3.6) viewed on the computer monitor was used during this test. The software, Infinite Analyze, provided with the Lumenera camera, has an option to create grid lines on an image (Figure 24). An image of the divisions of the calibration slide was captured and the reference grid line coinciding with a reference division bar on the image was noted. The stage was then moved in the x- direction a number of steps

and brought back the same number of steps. Another image was taken at this stage. If in this image, the reference division bar did not coincide with the reference grid line (as judged visually), the absolute value of the distance it shifted (Δx) was measured using the measurement option of the same software. The same test was repeated for the y-axis.

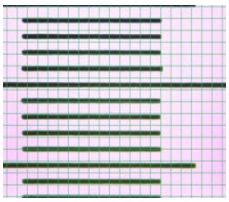

Figure 24: Reference grid line (green) on the division bars of the calibration slide

Results

The test was repeated 10 times for each distance. The difference measured for x- and y-axes are given in Table 9.

Table 9: Results showing the average shift in x- and y-axis movement

Distance moved µm	Mean difference (SD)	
	x-axis µm	y-axis µm
100	1.50(±2.51)	0.76(±0.85)
50	2.09(±2.64)	1.23(±1.36)
10	2.1(±2.06)	1.88(±1.62)
5	2.51(±1.43)	2.48(±1.41)

Discussion

The test results show that the motor attains the commanded position in both the axes without any large variability. The shift was higher for the smaller distances moved. However, it does not affect the study as the step sizes in x- and y- axes less than 50µm were not used in the study. Also, 50µm was a small area when compared to the total area of the field (see Section 7.6).

7.2.2 Accuracy of z-axis movement

Methods

The z-axis movement was investigated to determine whether there is any hysteresis in attaining the desired position using the focus motor, which would affect in the focusing of a field. For this purpose, the z-axis was sent a number of steps in one direction from the focus point and brought back to the focus point while capturing images at each position during its upward and downward movement through the same positions. The focus measures of the images were plotted against the position at which they were captured.

Results

The above test was repeated ten times. The average shift was calculated to be 0.00225µm. An example of the graphs obtained in the test is shown in Figure 25. The shift in focus, if present during the upward and downward motion of the z-axis through the same positions, was compared by super-imposing the graphs obtained.

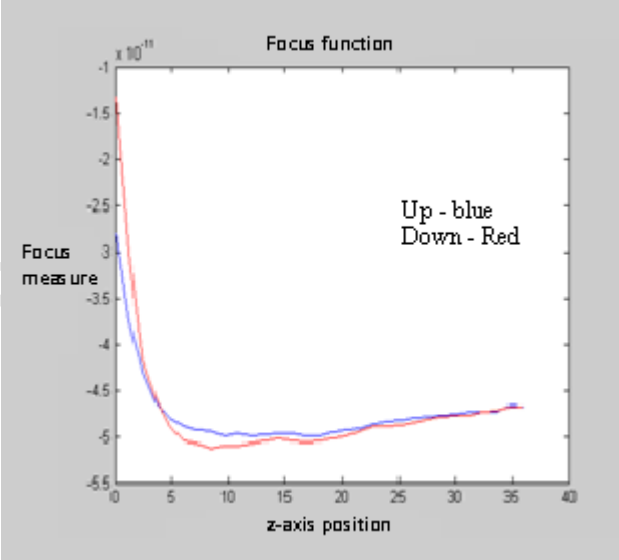

Figure 25: Focus function against z-position during upward and downward movement

Discussion

The average shift calculated shows that there is a negligible amount of hysteresis present in the z-axis movement and focus is unlikely to be affected.

7.3 Focal point variation in different slides

Methods

A test was conducted to determine if different slides had similar focal positions. Smear thickness as a result of smear preparation inconsistencies would result in different focal positions in different slides.

The objective position relative to the stage was kept constant throughout the experiment. Slides were loaded one after the other with no particular order followed. Each slide was brought to focus manually and removed without disturbing the z-axis position. The steps required to bring the first field of each slide to focus was noted.

Results

Fifty slides were tested in this experiment, both positive and negative slides. Results are shown in Figure 26.

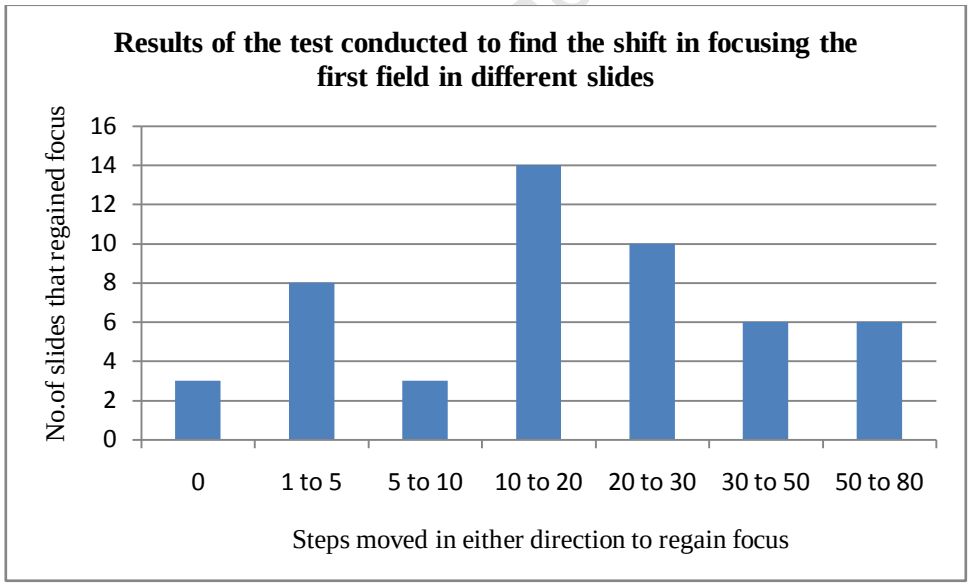

Figure 26: Focal point variation in a set of slides

Discussion

Figure 26 shows that the first field of some tested slides appear to be in focus only when 80 steps are moved in either direction along the z-axis. In practice, searching through such a large number of images in both directions would be time consuming and undesirable.

The results show a large amount of inconsistency faced in focusing on the first field of a new slide loaded on to the system. This would affect the auto-focusing implementation for the first field of different slides due to the large number of images having to be taken in a z-stack in order to estimate the focus. This project did not explore a solution for this problem; instead, manual focusing was done for the first field of all slides to test other components of the system.

7.4 Effects on focal position due to x- or y-axis movement

Tests were conducted to determine if x- y- movement of the hardware affected focus.

7.4.1 Test performed on the adapted Nikon 55i

Methods

From a focused field viewed on the computer screen, the stage was sent a certain distance along the x- and y- axes. The new field of view was refocused, if necessary, and the number of steps moved along the z-axis to bring the field to focus was noted. This test was done for increasing distances varying from 10µm to 160µm and 10µm to 120µm along x- and y- axes respectively to determine if the distance moved also affected the amount of defocus. The image size is 160µm and 120µm, and moving these distances along the x- and y- axis allowed adjacent fields to be reached without overlap.

Results

This test was performed on five different slides and the results obtained are given in Table 10 and Table 11. The test was repeated 10 times per distance and the mean was calculated.

Table 10: Effect of x-axis movement on focusing in Nikon55i microscope

Mean distance moved in x-axis µm	Steps moved to regain focus irrespective of direction (average of 10 repeated tests) 1step = 1.2µm					Mean
	Slide 1	Slide 2	Slide 3	Slide 4	Slide 5	
10	1.5	0.6	0.4	0.3	0.5	0.66
50	3.3	2.3	3.3	2.7	2.9	2.9
100	6.2	3.1	5.1	4.9	3.9	4.64
160	9.6	5	6.7	5.6	6.5	6.68

Table 11: Effect of y-axis movement on focusing in Nikon55i microscope

Mean distance moved in y-axis µm	Steps moved to regain focus irrespective of direction (average of 10 repeated tests)					Mean
	Slide 1	Slide 2	Slide 3	Slide 4	Slide 5	
10	0.4	0.1	0	0.3	0.1	0.2
50	0.3	0.4	0.1	0.3	0	0.22
100	0.9	0.6	0.2	0.1	0.1	0.38
120	0.5	0.2	0.1	0.5	0.1	0.3

Discussion

The results show that the effect of x-axis movement on focus is much higher than that of y-axis movement. The higher the distance moved in x-axis, the more steps were required to regain focus. To localise the problem the same test was performed on another microscope, as described in the next section.

7.4.2 Test on another microscope (Zeiss Axioskop2) for comparison

Methods

The test performed in the previous section was repeated on another microscope (Zeiss Axioskop2) using the same slide for both microscopes for comparison of the results.

Results

The highest distances during field-to-field movement (160µm for the x-axis and 120µm for the y-axis) were moved during the comparison test. The test was performed on one slide. The absolute distance and not the number of steps (1 step size is equal to 1.2 micrometers) is measured during this test because of the absence of a focus motor in the Zeiss microscope. The test was repeated 10 times. The results are given in Table 12.

Table 12: Comparison results of adapted Nikon microscope with Zeiss microscope

	Mean (SD) x-axis (160µm)	Mean (SD) y-axis (120µm)
Zeiss	0.74µm (±0.42)	1.43µm (±1.28)
Nikon	8.28µm (±4.5)	0.12µm (±0.38)

Discussion

The test result shows that the amount of defocus present when the x-axis is moved is low for Zeiss compared to the adapted Nikon microscope. The effect of y-axis movement on defocus is higher for the Zeiss Axioskop2 microscope. Further investigation into defocus due to x-axis movement is described below.

7.4.3 Further investigation into defocus due to x-axis movement

Methods

The reason for the high level of defocus due to x-axis movement in the Nikon microscope was investigated further. The amount of defocus due to x-axis movement was again tested and compared with Zeiss Axioskop2 microscope. Evenly distributed tissue slides were used in this experiment to eliminate the chances of an uneven smear affecting the shift in focal point while moving in the x-axis. In addition, the direction of focus motor movement to refocus was noted.

An area in the slide was marked to ensure that the same region was examined using both microscopes. The test conducted for the above two sections was repeated for this section from the marked position in the slides for both microscopes. If the fields were out of focus, the distance moved to bring those fields back to focus was noted for both microscopes and compared.

Results

The distance moved along the x-axis for this test was 1000µm. A higher distance was used as it may magnify the amount of defocus. Positive and negative signs were used to differentiate the direction of stage movement away from and to the objective, respectively, in regaining focus. The results are given in Table 13.

Table 13: Further investigation and comparison results on the effect on focus due to x-axis movement in Zeiss Axioskop and Nikon55i microscopes

	Distance moved along z-axis to regain focus (1000µm) (µm)					
	Zeiss Axioskop2			**Nikon 55i**		
	Slide 1	**Slide 2**	**Slide 3**	**Slide 1**	**Slide 2**	**Slide 3**
	0	0	0	0	0	0
	1.29	3.6	2.49	0	0	0
	0	-0.51	1.2	1.2	0	1.2
	1.72	0.60	-1.46	9.6	1.2	-1.2
	0	-1.72	-0.94	6	9.6	1.2
	0	0.43	0.51	0	0	9.6
	-0.34	0	-0.77	16.8	8.4	0
	0.95	1.20	1.46	9.6	19.2	8.4
	0.51	0	0	6	12	16.8
Mean (SD)	0.46 (±0.71)	0.4 (±1.4)	0.28 (±1.3)	5.5 (±5.8)	5.6 (±7)	4 (±6.2)

After moving the same distance along the same fields of an even smear using two different microscopes, the degree of defocus in the prototype microscope was still found to be higher than in the Zeiss microscope.

A common pattern observed in the results for the adapted Nikon is that, in most cases, the distance the stage was moved to refocus was in one direction i.e. away from the objective.

Discussion

The high defocus experienced along the x-axis could be due to the cantilever slide holder installed in the prototype. In this cantilever slide holder system the slide is held only at one end and not evenly supported. This may cause the slide to slant from the holder.

Figure 27 shows an illustration of the slide holder of the hardware system used in this project (see Section 4.3.1). It shows the direction in which the x-axis movement takes place in this hardware: towards the slide holder. This means that if there is a tilt present in the slide, because of gravity, with the free end of the slide further from the objective, then the objective and the distance between the slide decreases with an x-axis movement, and the stage would have to be moved away from the objective to regain focus, as found in the test. More stage movement away from the objective would be required for large x-axis distances moved.

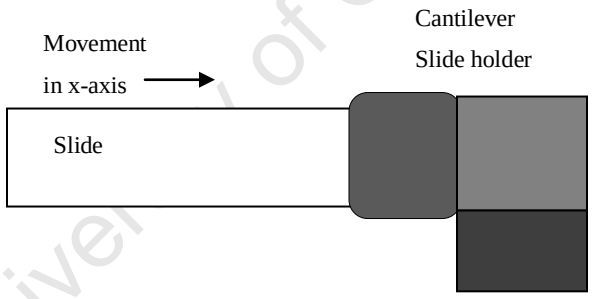

Figure 27: Illustration of the cantilever slide holder

7.5 Overlap of fields

Overlap between subsequent fields is advised during examination of a slide to eliminate the chances of missing any bacilli present on the border of two fields. But the amount of overlap between two fields can be increased or decreased taking into account other hardware characteristics such as processing time. In this case, the effect of x-axis movement on the focus as explained in the previous section, contributed to the determination of the amount of overlap between fields. The higher the amount of overlap

between two fields the shorter the distance moved from one field to another. A test performed to select the amount of overlap along the x-axis to eliminate the high degree of defocus associated with its movement is described below.

Methods

Stage movement in the y-axis did not affect the focusing algorithm as the degree of defocus found in the tests (Section 7.4.1) was low. Therefore, only a minimum overlap of 20% was introduced for y-axis movement to ensure that bacilli at the border of two fields would not be missed.

Since stage movement along the x-axis resulted in greater defocus when larger distances were moved, a test was performed to determine if a higher percentage of overlap, i.e. moving smaller distances, would result in less defocus.

Results

Three slides were tested 10 times per distance. The minimum, maximum and the mean number of steps required to regain focus in the 10 tests per distance are given in Table 14.

Table 14: Shift in focus relative to the percentage of overlap

Percentage of Overlap	Distance Moved µm	Steps moved to regain focus								
		Slide 1			Slide 2			Slide 3		
		Min	Max	Mean	Min	Max	Mean	Min	Max	Mean
20%	128	0	10	5.1	0	13	7.5	1	12	5.5
40%	96	1	8	5.1	0	11	6.4	1	8	5
50%	80	1	6	3.9	0	8	4.5	0	5	1.9
60%	64	1	5	2.8	0	6	4.1	0	5	3.3
70%	48	0	5	2.3	0	4	2.6	0	7	2.4
80%	32	0	5	2.7	0	5	2.4	0	4	1.5
90%	16	0	2	0.7	0	3	1.4	0	4	1.6

Discussion

The results show that the degree of defocus ranged between 0 and 13 steps for varying distances from 16 to 128µm. A larger overlap resulted in less defocus. However, large overlap would require more fields to be examined and therefore more fields to be processed, ultimately resulting in longer processing time.

The z-stack size depends on the level of defocus. The higher the defocus, the larger the number of images required in the stack and vice versa for effective auto-focusing. A 60% overlap was introduced for x-axis movement. With this percentage of overlap the maximum number of images taken in the stack to find the focal position in the test was six in both directions. But in the implementation, nine images were taken from both sides as smear thickness may also vary. This percentage of overlap was found empirically to overcome the effect of defocus during x-axis movement.

7.6 Determination of the number of fields to be examined

The location and size of smear samples are not consistent in slides as no standard position, size or shape is observed in the preparation of sputum smears. An optimal automated microscope with low processing time would be able to scan the entire slide. However, the prototype described here is still in a developmental stage, and scanning of the entire slide cannot be done quickly, because of mechanical stage movement.

Therefore, this project strove to meet the standard set by the WHO (Section 2.3) which is 100 fields examination for a 100 times magnified fields of view (World Health Organization, 2003). Since this study uses 40x magnification, a larger circular area can be viewed per field. Therefore, a smaller number of fields (N) viewed at 40x magnification would theoretically cover 100 fields viewed at 100x magnification and N is calculated here by the using the equation given below.

For an objective, with respect to its magnification, an estimate of the area covered by N circular fields of view is given by:

$$Area\ viewed\ per\ field = N\pi r^2$$

where r is the radius of the field viewed through a certain magnification and N is the number of fields, πr^2 gives the circular area viewed through an eyepiece.

For a 100x objective, N is 100 and the radius of the field of view of a 100x objective on the Nikon microscope was 110µm. The radius was measured using the micrometer slide (Section 4.3.6) placed under the objective and counting the number of divisions across the centre of the field (which gives the diameter) that can be viewed through the eyepiece. For an equivalent area to be viewed using the 40x objective, whose radius was

measured (using the same approach as mentioned for 100x) to be 280µm N, is approximately 15 without any overlap.

The camera used in this study does not capture the whole field area visible through the eyepiece. Only a smaller area of the field of view is captured in an image because of the crop factor (Section 4.3.4) of the Lumenera camera. The crop factor varies for different cameras. The area of a rectangular field that was obtained on a computer monitor through the image sensor was equal to 160µm × 120µm without any overlap. Figure 28 shows the measurement using a micrometer scale as obtained on screen.

(a) 160µm along x-axis **(b) 120µm along y-axis**

Figure 28: Calibration slide divisions showing the measure of length and breadth of a field captured by the camera

With this feature taken into consideration, the area viewed per image is much less than the actual 40x magnification field viewed through an eyepiece. To compensate for this, it was necessary that a higher number of fields be checked. The number of images that would meet the standard set by WHO for 100x magnification as mentioned before was calculated as given below. x is the number of images to be taken in this hardware to meet the area covered by 100 fields of 100x magnification.

$$100\pi r^2 = x \times area\ per\ image$$

$$x \cong 198$$

where 160µm × 120µm gives the area viewed per image. To meet the standard set by the WHO, 198 images without any overlap were required to be taken with this hardware.

Discussion

In Section 7.5 it was established that an overlap of 60% along the x-axis and 20% along the y-axis were required to avoid: a) missing any bacilli that may lie at the border of two images b) the degradation of images due to degree of defocus in this microscope system associated with x-axis movement. With this degree of overlap, a higher number of images should be taken to equal the area covered by 198 images.

Thus in this hardware, the number of images, to be captured with the introduction of overlap, to meet the WHO standard is very high. The pattern of field-to-field movement will affect the number of images required, because the percentage of overlap differs for the x- and y- axes. This is discussed in the following section.

7.7 Pattern of field-to-field movement

The field-to-field movement through the smear for TB detection can be effected in various ways. Patterns suitable for this study are explored below.

Methods

The defocus associated with the x-axis and the amount of overlap required for images taken after x-axis movement were established in the previous sections. Due to its impact on the quality of auto-focusing and the processing time, x-axis movement was limited. Therefore a higher number of field-to-field movements along the y-axis were established. The number of y-axis movements was determined by trial and error, to ensure the smear remained in view for different smear sizes.

Results

Thirty field-to-field movements were determined for the y-axis. The distance covered by 30 field movements with 20% overlap was 2880µm and was empirically found to be inside the smear from the start position (the start position is described in the next section). Movement along the x-axis took place every 30th field.

With 198 as the calculated number of fields to be processed (not considering the amount of overlap), the pattern of movement when implementing the above mentioned number of x- and y-axis movements is shown in Figure 29.

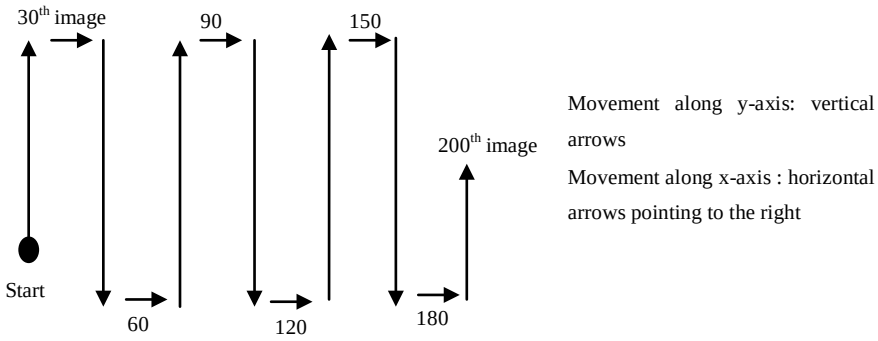

Figure 29: Pattern of stage movement on the slide to go through different fields

From the start position, 30 fields are processed in the y-axis in one direction (let's say upward direction), then the next field will be in x-axis (as shown in Figure 29) and then again 30 images in y-axis but in a downward direction and so on. If the y-axis was moved in only one direction, for example upwards, it would go out of the smear, hence movement in both directions was implemented. Figure 30 demonstrates how the required area is covered without overlap. The number of fields to be processed with the overlap derived in Section 7.5 and the pattern established in this section is shown in Figure 31. Approximately 619 overlapping fields are required to cover the same area as 198 non-overlapping fields.

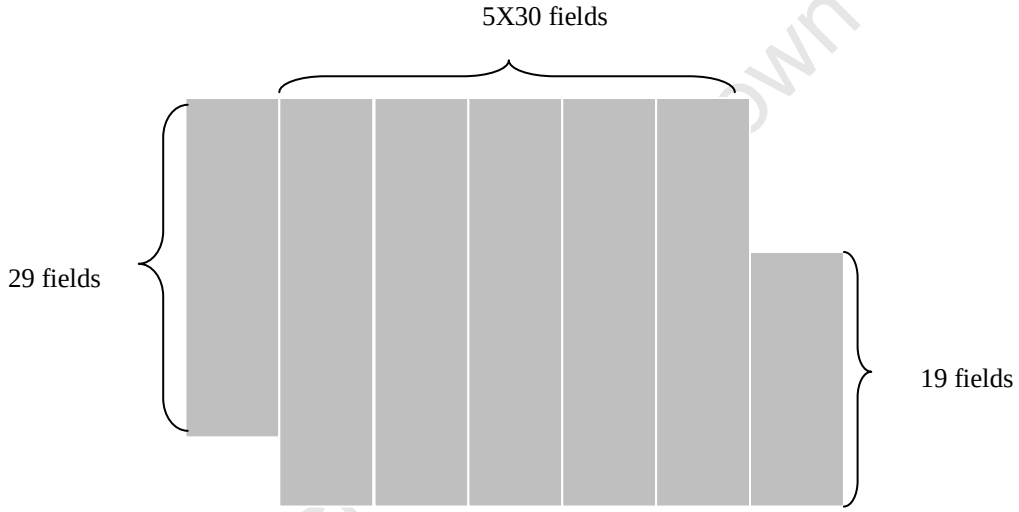

Figure 30: Number of fields covering an area as per the pattern followed for 198 fields

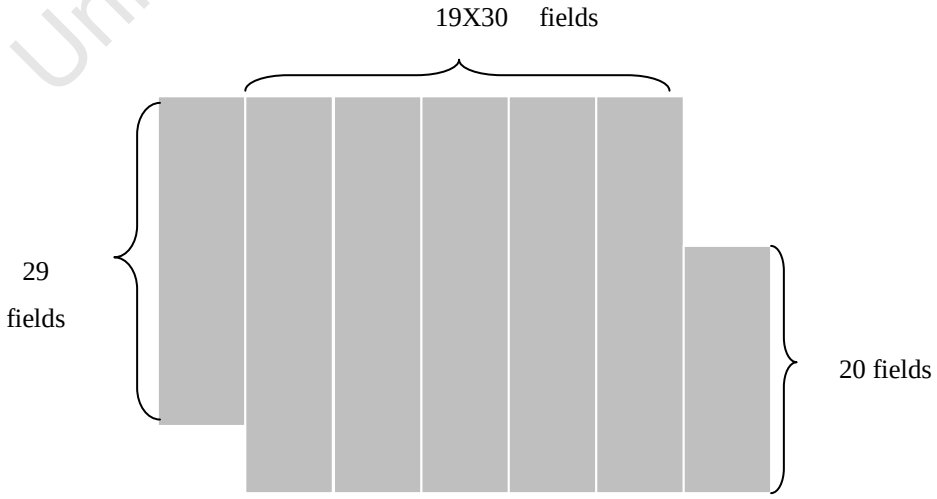

Figure 31: Number of fields (619) required to cover the area viewed without any overlap

7.8 Determination of the starting position of the scan

Scanning cannot be started from anywhere in the slide as the position may not be inside the smear or may be at the maximum distance that the motor can travel. The position to start the scanning process is determined in this section.

Methods

Every time a new slide was loaded the stage had to be positioned with respect to the objective so that the objective would view the smear. Therefore an absolute position to start a scan for a slide loaded was determined experimentally as below.

Note that the stage cannot be moved to a desired position manually (Section 4.3.2) due to the stage design of this hardware.

The layout of a typical TB sputum slide obtained from NHLS and used throughout in this study is shown in Figure 32. The total length of the slide is 76mm with a width of 26 mm and thickness of 1mm. For the linear actuator (Section 4.3.2) used in this project, the maximum distance that can be moved along the x- or y-axis is 28mm from the home position (H). The home position is approximately 22mm away from the left corner (facing the user) of the slide as shown in Figure 32. This position was measured using a ruler. The home position was set by previous researchers who designed the stage so that the smear is near this position and the entire smear falls within the 28mm x 28mm area that can be covered by the Zaber linear actuators used for the stage movement.

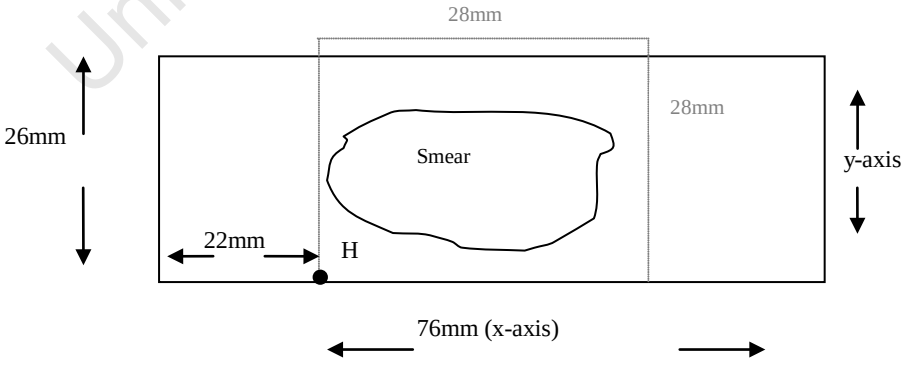

Figure 32: Layout of a typical TB sputum slide

The smear lies roughly at the centre of a slide, but its location is expected to differ in some cases because the position and shape of the samples on slides is not fixed. An experiment was conducted to find the absolute position on the slide where the smear would typically lie for a large number of fields.

With 1000µm increments in distance along the y- and x- axes respectively from the home position, the distance at which the smear could be viewed through the microscope for each slide was found and chosen as the start position for smear analysis.

Results

Sixty five slides were used for testing to determine this position. Figure 33 and Figure 34 show the results obtained while testing these slides to determine the start position for TB analysis.

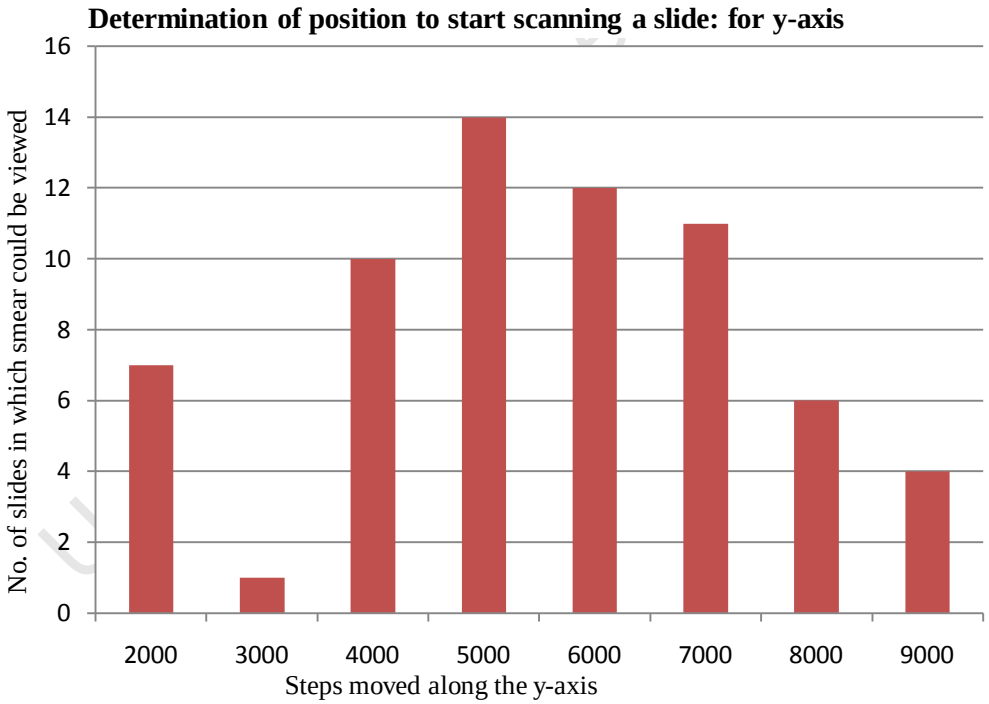

Figure 33: Results obtained for the determination of start scan position along the y-axis

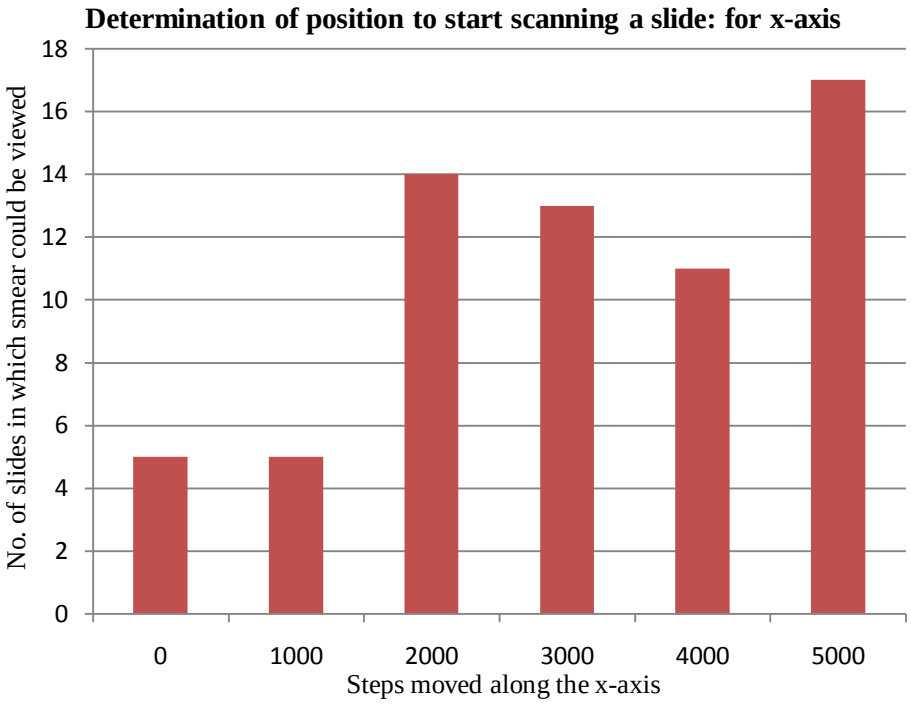

Figure 34: Results obtained for the determination of start scan position along the x-axis

Discussion

It was found that the objective fell over the smear within 9000 steps along the y-axis and within 5000 steps along the x-axis. Figure 35 illustrates the start position (S).

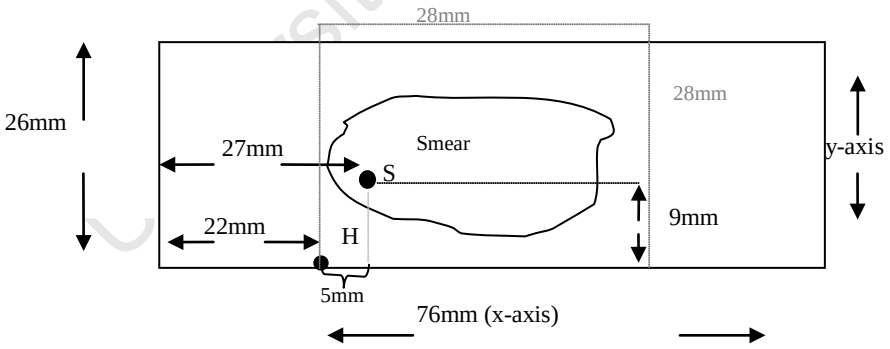

Figure 35: Illustration of the start position on the slide layout

The start position lies 6mm and 10.8mm from the home position along the x- and y- axes respectively. With the start position determined one does not have to manually look for a position to start the scan.

8. Integration - Methods

This section explains how the integration was performed to automate the system for TB bacillus detection in ZN-sputum smears. This chapter uses the results obtained from Chapter 6 and Chapter 7. Integration was performed by linking the auto-focus algorithm described in Chapter 5 and the software components described in Chapter 6 with the hardware described in Chapter 4, taking into account the characteristics of the hardware discussed in Chapter 7.

8.1 Introduction

System integration is a significant task which interfaces hardware and software components that function independently to work as an automated unit. Software that carries out a specific task correctly when offline, may not work perfectly when simply combined with the hardware and other software. This may be because of some unnoticed characteristics of the hardware or miscommunication with any of the other software components. Some additional hardware tests may therefore need to be performed once the components are interfaced.

The software components were developed in MATLAB and therefore software integration was carried out in MATLAB. The camera, focus motor and linear actuators for stage movement could already be operated independently from the MATLAB environment using the software provided by the supplier of each component. These software components along with the software for auto-focusing and pattern recognition were employed to meet the goal of the automation of the whole process of slide analysis with a single mouse click. A GUI was designed for human interaction with the hardware system.

8.2 Graphical User Interface

A GUI designed allows the user to perform the automated TB detection process. A user-friendly design was necessary for operators with varying computer skills. The GUI (features given in Table 15) was created in the interactive GUI design environment, in MATLAB.

Table 15: GUI features implemented and their associated functions

Main features in the GUI	GUI component	Function	When to operate
Open port	Push button	Opens the serial port connected to the motors	Once when the system is switched on after being completely shut down
Home stage	Push button	Sends the stage to default Home position	In case the stage needs to be send to default Home position
Position on smear	Push button	Positions the stage so that the objective lay over the smear	In case the process is interrupted and needs to start over
Start auto detection	Push button	Starts the automated TB detection process from focusing till the slide is identified positive or negative	After a slide has been loaded for TB bacillus detection
Image display	Axes	For displaying the original, corresponding segmented and classified images	For cross-checking or verification of any image
Enter image name	Edit text	To specify the image name of a certain slide and certain field to display	For cross-checking or verification of any image
Display	Push button	Displays the original, segmented and classified images of the name specified in the edit text	For cross-checking or verification of any image

8.2.1 Operator interaction

The operator is required to load a slide and manually focus the first field. Then the detection process can be started by clicking on the 'Start Auto Detection' button in the GUI. Then she/he is required to input two parameters listed in the next section.

8.2.2 Input parameters

An input dialog box appears once the 'Start Auto Detection' button is clicked. It requires the user to input the identification number of the slide before starting the process, in order to store the images with their associated slide number. The field number is attached to the image filename.

The second input parameter is the number of images to capture in the first stack. This was used during the development and testing of the system. It makes the system more

flexible in terms of focusing on the first field. If the user has focused the slide manually then she/he can enter a small number of images to capture in the first stack (four was the minimum number of images empirically found to be sufficient).

8.3 Integration route

The route taken to integrate some functions during the automation of the microscope for the detection of bacilli in 40x images of ZN-stained sputum smears is described in the following sections.

In some instances the implementation was different for the three cases: 1) the first field of a slide; 2) every field after y-axis movement; 3) every field after x-axis movement. Differences in implementation for the different cases are described in this section.

8.3.1 Taking a stack of images

A stack of images needed to be captured for auto-focusing. The software provided by Tofra focus-motor was used for stage movement.

As described in Section 7.3, manual focusing of the first field was required. The motor rests at the position at where the last image was captured. When the focus position is calculated using the auto-focusing algorithm, it is sent to that position and that becomes the new rest or start position. The start position is always the position of focus of the previous field or previous slide unless disturbed.

For the first field, even though manually focused, it is still advisable to perform auto-focusing. This is because manual focusing on a field is done while looking through the eyepiece and it was observed that the focus is not always optimal when the camera captures an image of the same field at that position. Also, it eliminates any human input error. Therefore four images were taken in the stack for auto-focusing on the first field. Manual focusing can be done by looking at the field from the monitor, which would eliminate this problem. But MATLAB cannot run simultaneously with the software to view the field in the monitor.

From the second field onwards, for every y-axis movement, curve-fitting was applied to reduce the time taken for focusing. Three images were captured around the focal

position of the previous field. Therefore the motor was moved once in one direction from the start position and then twice in the other direction.

For the field after x-axis movement, 18 images were taken in the stack. The focus motor was programmed to move half the number of steps (nine in this case) to one side, before changing direction to capture the desired number of images. This pattern ensures that all nine positions on both sides of the focal position of the previous field are covered.

8.3.2 Stage movement

Field-to-field movement was facilitated taking into account the results obtained from Section 7.5 and Section 7.7 in hardware testing. With a 20% overlap for every y-axis movement, 96µm was moved along the y-axis and with 60% overlap for every x-axis movement, 64µm was moved along the x-axis. The corresponding linear actuator is moved for every x- or y-axis movement using the software supplied by Zaber.

The stage is sent to the start position each time a slide is finished processing. Therefore, when a new slide is loaded, it is already positioned at the start position and scanning can be started at once.

8.3.3 Segmentation and classification

An image captured for an auto-focused field is segmented. Two conditions may occur after segmentation: 1) no objects are segmented in an image; 2) there are segmented objects.

When no objects are found in the segmented image, no further processing takes place and movement to the next field is effected. By doing this, classification of a segmented image with no objects is avoided, saving processing time. This was implemented using a nested loop inside the segmentation algorithm as shown in Figure 36. When there are objects present, the algorithm follows the usual path of classification, labeling and counting the classified objects.

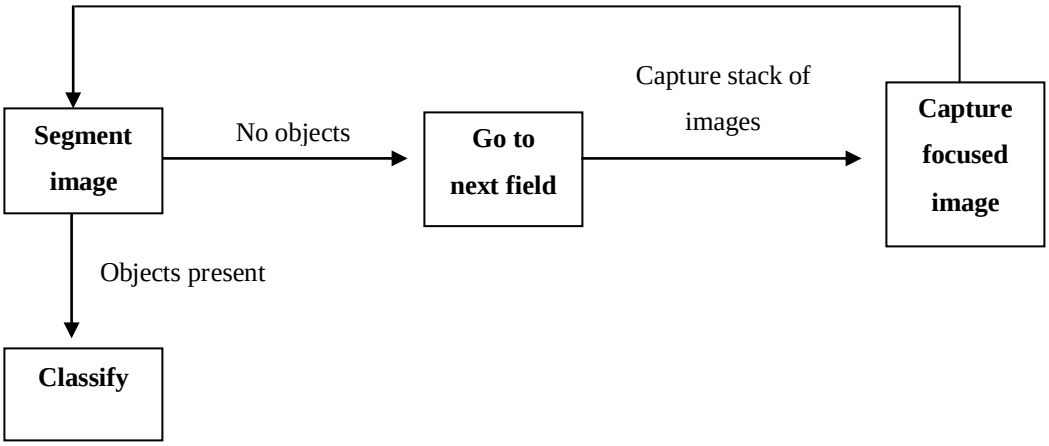

Figure 36: Segmentation implementation flow chart

8.3.4 Threshold set for determination of TB

The bacillus count per field and the cumulative count per slide are recorded. Based on this count the sputum smear is classified (refer to Table 1 for the grading). Therefore a counting system and a scanning process were implemented as given in Table 16.

Table 16: Threshold for the classification of a slide as TB positive or negative

Number of bacilli identified	Classification of the slide	Scanning process
0 in the whole slide	TB Negative	Scans all fields
<5 in total from all the fields checked	Can be a False Positive (shows the number of bacilli counted in the whole slide)	Scans all fields
5-99 in the whole slide	1+ TB Positive (shows the number of bacilli counted in the whole slide)	Scans all fields
1-10 per field	2+ TB Positive (shows the number of bacilli counted in the whole slide)	Stops scanning when the slide is identified to be 2+
>10 in one field	3+ TB positive (shows the number of bacilli counted in the whole slide till the field with more than 10 bacilli)	Stops scanning when more than 10 bacilli are detected in a field

If there is no bacillus identified during the scanning process, the system continues checking all the fields to ensure that it is not a false negative. If there are less than five bacilli found in all the fields, then it may be a false positive. This is based on the pattern observed with the results obtained from this system during this study and it may not be true for other systems. If the number of bacilli identified in the whole slide is less than 99, then the sample is classified to have 1+ TB infection. A slide is classified as 2+, when the average number of bacilli per field is greater than one. Once the slide is classified as 2+, further processing of the slide is no longer necessary. When a field with more than 10 bacilli is encountered, it is highly likely that the person has got 3+ TB infection. Therefore it is not necessary to go through the rest of the fields; this saves time.

8.3.5 Database

The focused, segmented and classified images are stored in specific locations accessible to the user, so that she/he can verify the results if needed. The stack of images taken for auto-focusing is over-written each time because of the limitation of memory space. The images stored have their respective slide and field numbers (e.g. Slide1_Field3 for the 3rd field of the 1st slide) as image name for verification. The results obtained for each slide is recorded in an excel sheet.

8.4 Testing

Once the components were interfaced, the system was tested on a few test environments. This was done to improve the implementation of software such as auto-focusing and stage movement as initial failures occurred during the developmental stage. It was made to work on the first test environment (using 15 fields) at a preliminary stage. A second and a third test environment of 200 and 620 fields respectively was set to just exceed the required fields calculated in Section 7.6 and 7.7. Once the system was working as expected, its sensitivity and specificity were evaluated.

Most of the evaluation on the performance of the system was based on the second test environment as the third test environment was time consuming. Examining the whole slide is ideal to avoid the occurrence of false negatives. However, processing time may

be extremely long in order to scan an entire slide with the limitations of the hardware used in this study. Hence, it was beyond the scope of this study to process all the fields in a smear.

8.4.1 Testing the integrated system

Testing is required to confirm that the integrated system is working correctly. The test had the following steps: initialise the automation from the GUI, auto-focus, capture and segment 40x magnification images of ZN-stained sputum smears, classify the segmented objects as bacilli or non-bacilli, move the stage to the next field of view if enough bacilli have not yet been identified for a 2+ or 3+ TB positive result; keep count of the number of bacilli identified through all the scanned fields and at the end display the result for the slide. Sensitivity and specificity for the whole system was calculated by testing a set of slides including both negative and positive for the second test environment. A specificity test was performed for the third test environment for a few slides.

9. Integration - Results

The integration phase took into account the characteristics of the hardware and interfaced the auto-focusing, segmentation and classification unit with the hardware and made it function as an automated system. The integrated scanning procedure is given in the flow chart in Figure 37.

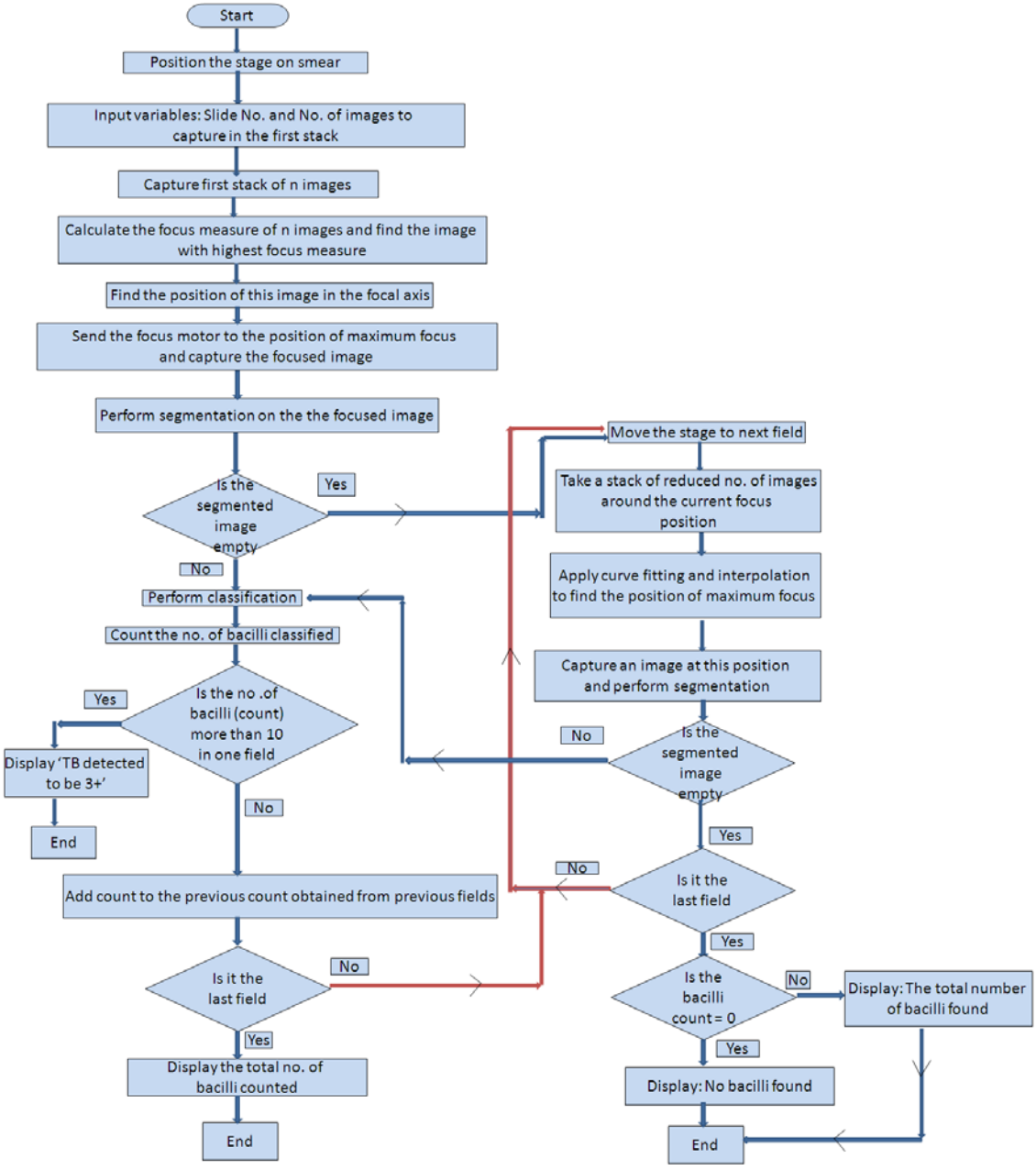

Figure 37: Flow chart of the integrated algorithm

9.1.1 Auto-focus implementation

Auto-focusing on the first field did not work well due to discrepancies in smear preparation and staining inconsistency (refer Section 7.3 for detailed information). Automating this part did not consistently produce focused images.

The stepper motor for z-axis movement in this microscope does not provide its position. If the z-axis motor provided position feedback, one might be able to find the range of focus for the first field on different slides. However, using the available hardware, it was necessary to do manual focusing for the first field of each slide as the focal point in each slide varies. Auto-focusing was performed after the initial manual focusing.

The auto-focusing implemented provided focused images of each field. Typical graphs obtained after the Vollath's F_4 based auto-focus implementation for the first field and for the curve fitting applied to a subsequent field are shown in Figure 38.

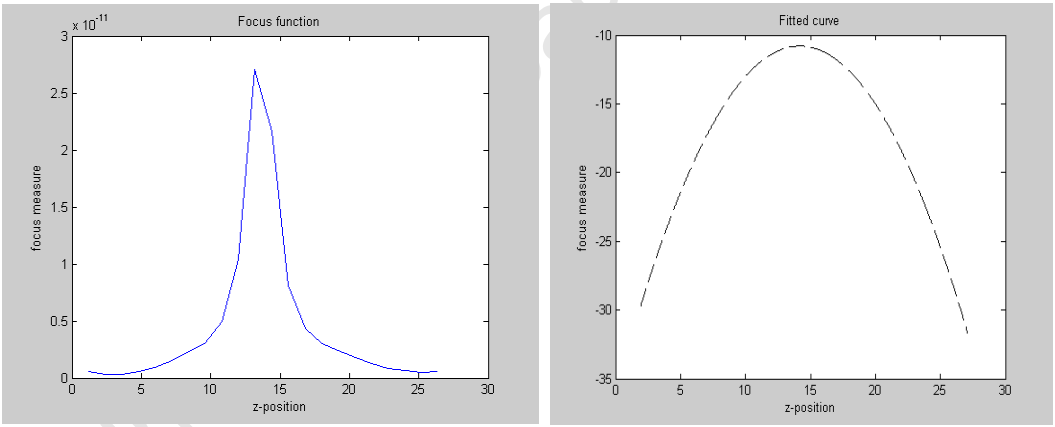

(a) **(b)**

Figure 38: Results obtained for auto-focusing implementation: a) Typical focus function plot obtained for first fields; b) Typical plot obtained when a quadratic curve is fitted for subsequent fields

The graphs have the shapes expected for a good focus measure. The peak of the curves gave the optimal focus position along the z-axis to where the focus motor is send to capture an image of the focused field. The resultant focused image is used in subsequent pattern recognition process.

9.1.2 Graphical User Interface

The GUI that was designed to allow the user to interact with the software for TB detection is shown in Figure 39 with the results displayed for TB positive and TB negative slides in Figure 40 and Figure 41. The input parameters required at the start of the slide processing is also shown in Figure 39. Examples of results displayed according to the threshold set are shown in Figure 42.

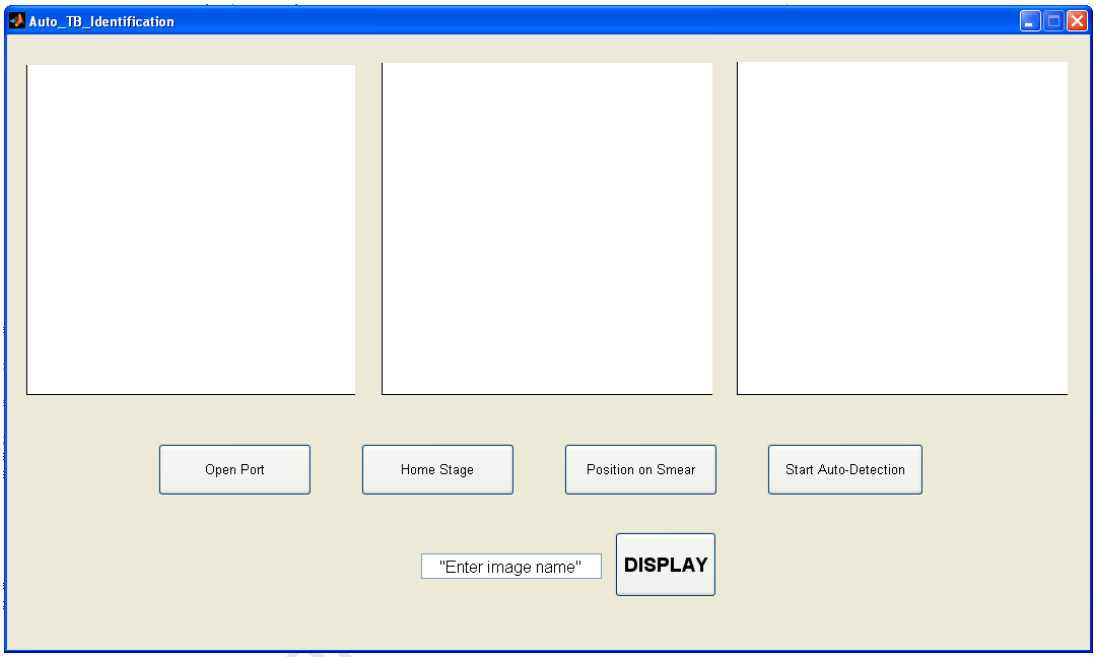

(a)

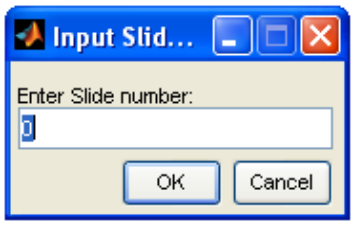

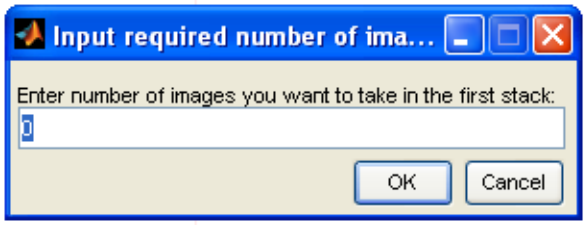

(b) **(c)**

Figure 39: a) the GUI that allows the user to start the TB detection process; b) Input parameter: Slide number; c) Input parameter: Number of images to capture for first field

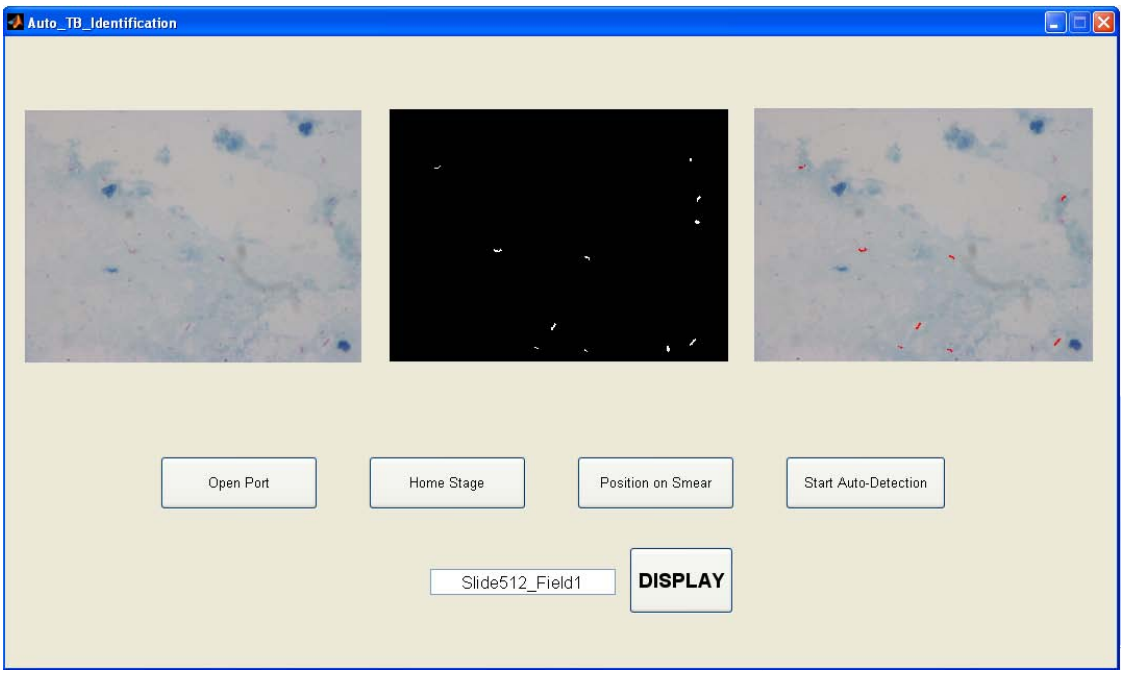

Figure 40: The GUI displaying the results of a TB positive image

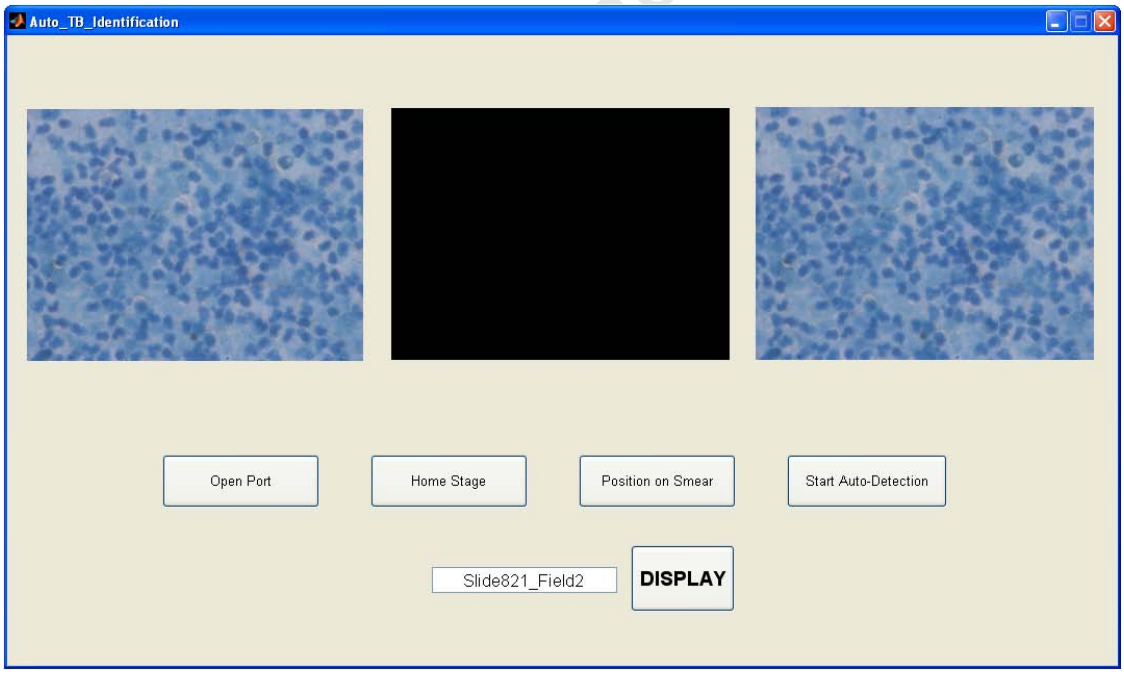

Figure 41: GUI displaying the results of a TB negative image

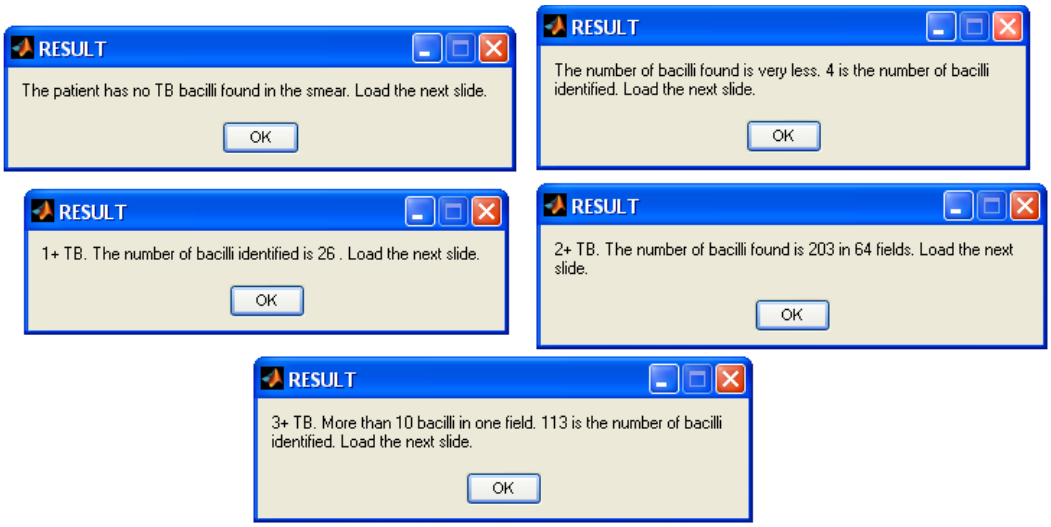

Figure 42: Examples of results obtained according to the threshold set

9.1.3 Time taken

The time taken for different functions is given in Table 17. The system typically took from 2.9 minutes to 12 hours depending on the number of objects segmented in an image to process 650 fields in a slide. To capture 10 images in a stack, it took an average of 76.48 seconds. The stacks that contained three images took an average of 29.3 seconds. Segmentation of a field took an average of 28.62 seconds. Time taken for the classification stage varied depending on the number of objects segmented in an image. On an average, it took 1.14 seconds to classify one object. The mechanical stage movement took approximately 2.95 seconds to go to the next field along the y-axis (96µm) and approximately 2.9 seconds along the x-axis (64µm). Capturing a stack of images along the z-axis took the longest time due to the mechanical motion of the z-axis motor through different focal points. In practical auto-focusing applications, the time taken for the mechanical motion of the objective with respect to the stage is the greatest source of delay (Subbarao and Tyan, 1998). For high throughput applications, image-based auto-focusing may be prohibitively slow since the acquisition of multiple images increases the total scan time (Yazdanfar et al., 2008).

Table 17: Time taken for the main functions

Function	Average time taken
Automated system	2.9 minutes to 12 hours
Capturing 10 images in a stack	76.48 seconds
Capturing 3 (minimum) images in a stack	29.3 seconds
Segmenting a field	28.62 seconds
Classifying an object in an image	1.14 seconds
Stage movement to go to next field (y-axis)(96µm)	2.95 seconds
Stage movement to go to next field (x-axis)(64µm)	2.9 seconds

9.2 Sensitivity and specificity

Fifty positive slides and 66 negative slides were processed for 200 fields. On an average, it took three hours 40 minutes to process one slide through 200 fields. Sensitivity was 92% and specificity was 89%. Ten negative slides were processed for 620 fields. All 10 tested negative. It took roughly 12 hours to process each slide.

9.3 Summary

A summary of the selected methods used to perform various functions in the automation of ZN-stained sputum smear microscopy for TB detection is given in Table 18.

Table 18: Various functions and the selected methods for integration; the sensitivity and specificity obtained for the integrated system are given in the last row

Function	Selected Methods
Auto-focus	Vollath's F_4 implemented with curve-fitting
Segmentation	Quadratic pixel classifier
Classification	kNN classifier
Stage Movement	96µm along y-axis and 64µm along x-axis
Number of fields to scan to meet WHO standards using the in-house hardware	620 fields
Sensitivity and specificity achieved for the integrated system	92% and 89%

10. Discussion, Conclusion and Recommendations

10.1 Discussion and Conclusion

The aim of the study was to develop a complete automated system for the detection of TB in ZN-stained sputum smears.

This project integrated auto-focusing and pattern recognition algorithms developed by previous researchers. The characteristics of the hardware were analysed for integration of hardware and software. The microscope can be controlled from a computer by an interactive graphical user interface that was developed in this study. Once the slide is loaded and manually brought to focus the first field, the user can perform the slide scan from the GUI on a single click, and by entering the slide identification number. The procedure then continues without human intervention and the results will be displayed on the screen.

The following difficulties were encountered in this project.

- A limited number of well-smeared and well-stained slides were available.
- Inconsistency in smear thickness on slides affects the performance of the algorithms and the system. For example, an uneven smear can affect the auto-focusing to an extent where the subsequent fields are unable to regain focus.
- The inter-dependency of algorithms created difficulties whereas each algorithm worked well independently. If the output of one function is incorrect, it affects the performance of consecutive functions.
- Hardware limitations that were observed during the integration of the software created difficulties and resulted in long processing time.

The images used to train and test classifiers were not the same as those used by Khutlang (2009). He obtained 100x magnification images from a high-end microscope. Digital cameras capture and register images differently and the colour, contrast and sharpness may vary in the images captured from different cameras. The images used for his study had a higher clarity and sharpness compared to the images used in this study. However, since in this study, the classifiers were trained using the images obtained from the same camera, it did not have a high impact on the segmentation and classification results.

Classification obtained good results that are comparable with related research. An accuracy of 97.05% with a sensitivity of 98.31% and specificity of 94.52% was obtained for the kNN classifier during cross validation and is comparable to the 98.55% accuracy, 97.77% sensitivity and 99.13% specificity obtained by Khutlang et al. (2010). Classification results may improve with better image quality as the objects would then retain a better boundary shape.

Hardware limitations affected auto-focusing implementation. The microscope stage with the cantilever slide holder is a unique feature of the system. This was implemented to make the system cost-effective. The auto-focusing algorithm worked correctly when tested offline on a set of images but the implementation of stage movement along with it created initial difficulty in obtaining focused images of fields, due to tilted slides. The x-axis movement was therefore limited and a higher overlap was introduced when the stage moved in the x-axis. There was a resultant higher processing time for the overall system.

The focus level for the first field in different slides was very different. This may be because of the unevenness of the smear and stain. Manual focusing of the first field was used; therefore one cannot say the final system is fully automated. In the literature (Allen et al., 2006; Mc Keogh et al., 1995), the initial focus in an automated microscopy for some applications is achieved manually.

Moreover, slide loading is not automated, as the slide has to be loaded manually.

The camera used in this study does not reproduce the clarity of a field as observed through the eye-piece. Even the best focused image does not appear very sharp. The colour properties of the camera used here were fixed and this may have affected the digital images captured from different fields. A method to vary the parameters of the camera according to different fields may be useful to acquire better quality images. The Abbe limit, which depends on wavelength and NA, limits resolution (Kino and Mansfield, 1991) and may have affected bacillus detection. Higher clarity of images would produce better segmentation and classification results, although the classifiers will need re-training with objects obtained from those images. The camera also does not reproduce the exact area of field of view as viewed through the eye-piece due to the effect of the crop-factor associated with the camera sensor. This hinders the purpose of

using 40x objective because more images were required to cover an area equal to images captured using a 100x objective, but could be overcome with the use of a different camera.

An algorithm can be implemented to see if the objective covers the smear by checking the properties of an image. Images of the smear will typically have a blue background and images of outside the smear will have a white background. Searching for such images may be expensive in terms of time and would require focused images of all fields that are scanned through till the smear is found. Therefore the system was implemented to start the scanning from a predetermined position obtained from a trial and error testing method.

Ideally, to achieve the most accurate results, especially in smears with sparse bacilli, the whole slide should be examined. This was not implemented in this study due to constraints on stage movement.

The grading system according to the WHO standards implemented in this study does not account for false positives and false negatives.

The system gave a satisfactory overall sensitivity and specificity although the processing time was high for processing a slide, especially in the case of sparse and negative slides (roughly about 12 hours). This makes the system not feasible to replace technicians who are expected to take around five (Cambanis et al., 2007) to 15 (Sadaphal et al., 2008) minutes per slide. A full-time technician should be able to scan around 20 (Cambanis et al., 2007) to 40 (Toman, 2004) TB slides per day whereas this prototype will be able to scan fewer slides depending on whether they are negative or positive. However, the microscope is only a prototype which can be improved further to achieve better throughput for slide scanning. Also, processing time on an average was 1.14 minutes per image depending on the amount of information present in an image. Therefore, when looked at on a per field basis, the automated system, with a more efficient mechanical system and a faster processor, may be a feasible cost-effective method for TB detection.

Newer diagnostic methods for TB use protein biomarkers, DNA amplification (PCR based methods) and fall under the broad category of molecular diagnostics. They are more sensitive and accurate, and can additionally give information on drug resistance, whereas smear microscopy does not. However, they are currently more expensive.

Therefore an initial screening by sputum smear microscopy could possibly reduce the diagnostic costs, provided false negatives are limited.

10.2 Recommendations

Segmentation and classification performance can be further improved by adding more datasets of higher variability by careful selection of the training set of both.

Standardisation of slide preparation would have advantages in terms of smear location. Standard TB slides would have a standard boundary area marked inside the slide where technicians should smear the sputum. With this feature, the system can be set to automatically scan that area and hence processing the whole smear can be achieved in case of negative or sparse bacilli slides.

Staining consistency would improve pattern recognition and detection of TB in ZN-stained sputum. It is recommended that the staining procedure be automated to avoid human-introduced inconsistency, for evenly smeared samples with good staining that gives a good contrast between bacilli and the background.

Homogeneity of the illumination system and characteristics of the optical system can be optimised to improve the image quality that may contribute to better pattern recognition results for ZN-stained bacilli identification.

The cantilever slide holder system should be replaced or corrected to ensure better auto-focusing. A better camera should be used to improve image quality and to increase the area viewed at per field.

Conversion of all software to a more efficient programming language such as C++ should be implemented to reduce processing time. Further time gains may be achieved by implementing the algorithms in a parallel processing environment.

References

Allen G P, Hodgson R M, Marsland S R, Arnold G, Flemmer R C, Flenley J, Fountain D W, 2006, 'Automatic Recognition of Light Microscope Pollen Images', *Image vision and computing New Zealand, IVCNZ 06 proceedings*, 355-360

Applied Scientific Instrumentation, 2003, Comparison of ASI's Closed-loop DC Servomotor Stages and Control Electronics with Competing Products, *Technical* Note 107, http://www.asiimaging.com/pdfs/Comparison_of_ASI_Stages_to_ Competitors.pdf Last date accessed: 23 May 2010

Baluja S, 1994, 'Population based incremental learning: A Method for Integrating Genetic Search Based Function Optimization and Competitive Learning', Technical Report CMU-SC-94-163 Department of Computer Science, Carnegie-Mellon University

Cambanis A, Ramsay A, Wirkom V, Tata E, Cuevas L E, 2007, 'Investing Time in Microscopy: An Opportunity to Optimise Smear-Based Case Detection of Tuberculosis', *International Journal of Tuberculosis and Lung Diseases*, 11(1), 40-45

Chang A R, Lin W F, Chang A, Chong K S, 2002, 'Can Technology Expedite the Cervical Cancer Screening Process', *American Journal Clinical Pathology*, 117, 437-443

Dendere R, 2009, 'Segmentation of Candidate bacillus Objects in Images of Ziehl-Neelsen Stained Sputum Smears using Deformable Models', *M.Sc Thesis*, Department of Biomedical Engineering, University of Cape Town

Duda R, Hart P, Stock D, 2001, 'Pattern Classification', John Wiley, New York:

Floyd A D, 1998, 'Automated Microscopy', *A workshop presented at the National Society for Histotechnology*

Forero M, Sierra E, Borrego A, Pech J L, Cristobal G, Alcala L, Desco M, 2001, 'Automatic sputum colour image segmentation for tuberculosis diagnosis', *SPIE Proceedings,* 4471, 251-261

Forero M, Cristobal G, Desco M, 2006, 'Automatic Identification of Mycobacterium Tuberculosis by Gaussian Mixture Models', *Journal of Microscopy,* 223, 120-132

Franco A, Lumini A, Maio D, Nanni L, 2006, ' An Enhanced Subspace Method for Face Recognition', *Pattern Recognition Letters,* 27, 76 - 84

Friedman M, Kandel A, 2000, 'Introduction to pattern recognition: Statistical, Structural, Neural and Fuzzy logic approaches', Imperial College Press, London

Fukunaga K, 1990, 'Introduction to Statistical Pattern Recognition', Academic Press, San Diego

Fundamental Optics, 2009, *CVI Melles Griot, Technical Guide,* 2, http://www.cvimellesgriot.com/products/Documents/TechnicalGuide/fundamental-Optics.pdf Last date accessed: 12 February 2011

Geusebroek J, Cornelissen F, Smeulders A, Geerts H, 2000, 'Robust autofocusing in Microscopy', *Cytometry,* 39, 1-9

Global Health Initiative, 2007, Investing in Global Health Research: Government should play a larger role, *A Global Health Initiative Fact Sheet, http://www.familiesusa.org/issues/global-health/government-funding.PDF* Last accessed on 24 February 2010

Gonzalez R C, Woods R E, Eddins S L, 2004, 'Digital Image Processing Using MATLAB', Prentice Hall, New Jersey

Hanscheid T, 2008, 'The future looks bright: low-cost fluorescent microscopes for detection of *Mycobacterium tuberculosis* and *Coccidae*', *Transactions of the Royal Society of Tropical Medicine and Hygiene*, 102, 520-521

Hatiboglu C U, Akin S, 2004, 'A new computerized moving stage for optical microscopes', *Computers & Geosciences*, 30(5), 471-481

Holdaway C A, 2004, 'Automation of pollen analysis using a computer microscope', *M.Sc Thesis*, Department of Computer Systems Engineering, Massey University

Huang W, Jing Z, 2007, 'Evaluation of focus measures in multi-focus image fusion', *Pattern Recognition Letters*, 28, 493-500

Huttenlocher D P, Klanderman G A, Rucklidge W J, 1993, 'Comparing Images Using the Hausdorff Distance', *IEEE Transactions on Pattern Analysis and Machine Intelligence*, 15(9), 850-862

ImageJ, 2009, ImageJ for microscopy, *Image Processing and Analysis in Java*, http://www.macbiophotonics.ca/imagej/ Last date accessed: 12 November 2010

Jerome J, 2010, 'Virtual Instrumentation using LabVIEW', PHI Learning, New Delhi

Khutlang R, Krishnan S, Dendere R, Whitelaw A, Veropoulos K, Learmonth G, Douglas T S, 2010a, 'Classification of Mycobacterium tuberculosis in Images of ZN-Stained sputum Smears', *IEEE Transaction on information technology in biomedicine*, 14(4)

Khutlang R, Krishnan S, Whitelaw A, Douglas T S, 2010b, 'Automated detection of tuberculosis in Ziehl-Neelseen stained sputum smears using two one-class classifiers, *Journal of Microscopy*,237, 96-102

Khutlang R, 2009, 'Image Segmentation and Object Classification for Automatic detection of Tuberculosis in Sputum Smears', *M.Sc Thesis*, Department of Biomedical Engineering, University of Cape Town

Kino G and Mansfield S, 2001, "Near field and solid immersion optical microscope". *United States Patent* 5004307

Luna J A C, 2005, 'A tuberculosis guide for specialist Physicians', International Union Against Tuberculosis and Lung Disease, Paris

Macedo M P, Barata A J, Fernandes A G, Correia C M, 2005, 'A wide-field microscopy technique using a linear image sensor for obtaining 3D images', *Proeedings of SPIE*, 570,172-180

Malik A S, Choi T S, 2008, 'A novel algorithm for estimation of depth map using image focus for 3D shape recovery in the presence of noise', *Pattern Recognition*, 41(7), 2200-2225

Mckeogh L F, Sharpe J P, Johnson K M, 1995, 'A low cost automatic translation and auto-focusing system for a microscope', *Measurement Science & Technology*, 6(5), 583-587

Mea V D, Viel F, Beltrami C A, 2005, 'A Pixel-based Autofocusing Technique for Digital Histologic and Cytologic Slides', *Computerized Medical Imaging and Graphics*, 29, 333-341

Meurie C, Lebrun G, Lezoray O, Elmoataz A, 2003, 'A Comparison of Supervised Pixel-Based Colour Image Segmentation Methods. Application in Cancerology', *WSEAS Transactions on Computers, special issue on ICOSSIP'03*, 2, 739-744

Mindru F, Tuytelaars T, Van Gool L, Moons T, 2004, 'Moment Invariants for Recognition under Changing Viewpoint and Illumination', *Computer Vision and Image Understanding*, 94, 3-27

Nicolls F, 1995, 'The Development of a Predictive Autofocus Algorithm using a General Image Formation Model', *M.Sc Thesis*, University of Cape Town

Nikon MicroscopyU, 2010, Articles – Formulas, http://www.microscopyu.com/articles/formulas/ Last accessed on: 24 January 2010

Olympus, 2010a, Basic Concepts in Light Microscopy, http://www.olympusmicro.com/primer/anatomy/anatomy.html Last date accessed: 9 August 2010

Olympus, 2010b, Basics of Light Microscopy Imaging, *GIT VERLAG*, http://www.aomf.ca/pdfs/OlympusGitVerlag_Basics.pdf Last date accessed: 25 August 2010

Ortiz-de-Solorzano C, Pengo T, Galarraga M, Muñoz-Barrutia A, 2008, 'Automation of the detection of lung cancer cells in minimal samples of bronchioalveolar lavage', *Proceedings of the IEEE Symbosium on Biomedical Imaging: From Nano to Macro*, 312-315

Osibote O A, Dendere R, Krishnan S, Douglas T S, 2010, 'Automated Focusing in Bright-Field Microscopy for Tuberculosis Detection', *Journal of Microscopy*, 240(2),155-156

Pal N. R, Pal S. K, 1993, 'A Review on Image Segmentation Techniques', *Pattern Recognition*, 26(9), 1277-1249

Pressman R S, 2005, 'Software engineering: A Practitioner's approach', McGraw-Hill, New York

Russell M, Douglas T S, 2007, 'Evaluation of autofocus algorithms for tuberculosis microscopy', *Conference Proceedings IEEE*, 3489-3492

Sadaphal P, Rao J, Comstock GW, Beg MF, 2008, 'Image Processing Techniques for Identifying *Mycobacterium Tuberculosis* in Ziehl-Neelsen Stains', *International Journal of Tuberculosis and Lung Disease*. 12(5), 579-582

Santos A, Ortiz de Solorzano C, de la Pena J, Vaquero J, Malpica N, del Pozo F, 1997, 'Evaluation of autofocus functions in molecular cytogenetic analysis', *Journal of Microscopy*, 188, 264-72

Shamir L, Delaney J D, Orlov N, Eckley D M, Goldberg I G, 2010, 'Pattern recognition software and techniques for biological image analysis', *PLos Computational Biology*, 6(11)

Sonka M, 2008, 'Image Processing, Analysis and Machine Vision', Thompson, Toronto

Steingart K R, Henry M, Ng V, Hopewell PC, Ramsay A, Cunningham J, 2006, 'Fluorescence Versus Conventional Sputum Smear Microscopy for Tuberculosis: A Systematic Review', *Lancet Infectious Diseases*, 6(9), 570-81

Sun Y, Duthaler S, Nelson B J, 2004, 'Autofocusing in computer microscopy: selecting the optimal focus algorithm', *Microscopy Research and Technique*, 65(3), 139-149

Subbarao M, Tyan J K, 1998, 'Selecting the Optimal Focus Measure for Autofocusing and Depth-from-Focus', *IEEE Transactions on Pattern Analysis and Machine Intelligence*, 20(8), 864-870

Svahn F, 1996, 'Tools and Methods to Obtain a Passive Autofocus System', *M.Sc Thesis*, Tekniska Högskolan Linköping

Takahashi K, 2007, 'Restoration of images with missing pixels', *Wiley Periodicals*, 22(2), 34-41

Thigpen J, Merchant F A, Shah S K, 2010, 'Photometric calibration for quantitative spectral microscopy under transmitted illumination', *Journal of microscopy*, 239(3), 200–214

Todar K, 2009, Mycobacterium Tuberculosis and Tuberculosis, *Todar's Online Textbook of Bacteriology*, http://www.textbookofbacteriology.net/tuberculosis.html Last date accessed: 24 September 2010

Tofra, 2010, Focus Drives, *Low cost components for Microscope automation*, http://www.tofrainc.com Last date accessed: 19 November 2010

Toman, 2004, Toman's Tuberculosis Case Detection, Treatment and Monitoring: Questions and Answers, World Health Organization, Geneva

Van den Doel L R, Klein A D, Ellenberger S L, Netten H, Boddeke F R, Van Vliet L J, Young I T, 1998, 'Quantitative evaluation of light microscopes based on image processing techniques', *Bioimaging*, 6, 138-149

Veropoulos K, Learmonth G, Campbell C, Knight B, Simpson J, 1999, 'Automated Identification of Tubercle Bacilli in Sputum: A Preliminary Investigation', *Analytical and Quantitative Cytology and Histology*, 21(4), 277-281

Veropoulos K, 2001, 'Machine Learning Approaches to Medical Decision Making' *PhD Thesis*, Department of Computer Science, University of Bristol

Wah T D, Wises P K, Butch A W, 2005, 'Analytic Performance of the iQ200 Automated Urine Microscopy Analyzer and Comparison With Manual Counts Using Fuchs-Rosenthal Cell Chambers', *American Society for Clinical Pathology*, 123, 29-196

Vollath D, 1988, 'The influence of the scene parameters and of noise on the behaviour of automatic focusing algorithms', *Journal of microscopy*, 151, 133-146

World Health Organization, 1998, 'Microscopy: Part II', *Laboratory Services in tuberculosis control*, WHO/TB/98.258. Geneva, Switzerland

World Health Organization, 2009a, 'Global Tuberculosis Control', WHO, Geneva

World Health Organization, 2009b, Tuberculosis Facts, Stop TB Partnership, http://www.who.int/tb/publications/2009/tbfactsheet_2009update_one_page.pdf Last accessed on 2 December 2009

World Health Organization, 2003, Supporting Laboratory Services, http://whqlibdoc.who.int/hq/2003/WHO_CDS_TB_2002.310_mod9_eng.pdf Last date accessed: 2 January 2010

Yazdanfar S, Kenny K B, Tasimi K, Corwin A D, Dixon E L, Filkins R J, 2008, 'Simple and robust image-based autofocusing for digital microscopy', *Optics Express*, 16(12), 8670-8677

Young I T, Zagers R, van Vliet I J, Mullikin J, Boddeke F, Netten H, 1993, 'Depth of focus in microscopy', Proceedings SCIA'93, Tronto, Norway, 493-498

Zaber Technologies, 2011, Actuator Characterization, *Technical Notes*, http://www.zaber.com/applications/?tab=Tech%20Notes&article=characterization Last date accessed: 11 January 2011